2017•2018

Faculteit Industriële ingenieurswetenschappen

master in de industriële wetenschappen: nucleaire technologie

Masterthesis

Radiological and non-radiological environmental impact assessment of Estonian power plants

PROMOTOR :

Prof. dr. Wouter SCHROEYERS

PROMOTOR :

Dhr. Tim VIDMAR

Wouter Slechten

Scriptie ingediend tot het behalen van de graad van master in de industriële wetenschappen: nucleaire technologie, afstudeerrichting milieutechnologie-radiochemie

Gezamenlijke opleiding UHasselt en KU Leuven

2017 • 2018

Faculteit Industriële ingenieurswetenschappen

master in de industriële wetenschappen: nucleaire technologie

Masterthesis

Radiological and non-radiological environmental impact assessment of Estonian power plants

PROMOTOR :

Prof. dr. Wouter SCHROEYERS

PROMOTOR :

Dhr. Tim VIDMAR

Wouter Slechten

Scriptie ingediend tot het behalen van de graad van master in de industriële wetenschappen: nucleaire technologie, afstudeerrichting milieutechnologie-radiochemie

UHASSELT KU LEUVEN

Prologue

As a master student at UHasselt, in the department Industrial engineering sciences – Nuclear Technologies Environmental Sciences – Radiochemistry, my interest into atmospheric modeling was first peeked in my bachelor project in which I used the rules of Thumb model into modeling different situations for atmospheric dispersion. Continuing this trend I was given the opportunity by the SCK-CEN (Studiecentrum voor kernenergie-Centre d'étude de l'énergie nucléaire), situated in Mol (Belgium) to do further research into atmospheric dispersion.

Firstly I want to thank both my promotors, dr. Tim Vidmar and prof. dr. Wouter Schroeyers, for the aid and assistance during my master thesis. I would also like to thank the Estonian colleagues Taavi Vaasma, Marko Kaasik and Alan Tkaczyk as their previous research as well as guidance throughout this research was very helpful. I also want to thank the SCK-CEN for giving me the opportunity to conduct this research.

Table of Contents

1. List of Tables

2. List of figures

3. Abstract

It is common knowledge that our environment is slightly radioactive, this includes our atmosphere. Coincidently the atmosphere is also an ideal environment for the distribution of natural and artificial radionuclides from place to place.
According to previous studies the oil shale industry is the largest producer of NORM (Naturally Occurring Radioactive Materials) waste in Estonia. With an estimated 11-12 million tons of oil shale containing various amounts of natural radionuclides which is burned annually in the Narva oil shale-fired PPs (power plants). This combustion process accounts for 90% of the Estonian electricity production.
This research focused on evaluating several models to predict radionuclide concentrations around coal PPs. These models include WESTIGAUSS, AEROPOL and IFDM.
In addition to fly ash emissions caused by the burning of shale oil, radionuclides found in oil shale remain attached to various ash fractions at ash separation points and are consequently emitted together with these fly ash fractions that escape the purification systems. Soils near the PPs have been found to contain elevated concentration of ^{226}Ra and ^{210}Pb. Recent studies have also shown that the atmospheric ^{210}Pb activity has a high variability in weekly, seasonal and yearly values.
The gathered results of the WESTIGAUSS (WE STIck to GAUSS) model, used by the SCK-CEN, to the AEROPOL results as well as a third model, namely the IFDM (immission frequency distribution model) were compared amongst each other. All these results were also compared to snow measurements taken in Estonia.
The IFDM model predicted an average snow deposition of 11,63 mg/m².d while the average measured snow deposition is 31,83 mg/m².d, it also showed a very bad correlation to the snow measurements. Therefore it was disregarded for further simulation.
The original WESTIGAUSS code was successfully extended to include three new features: treatment of multiple sources (and therefore sources that are not centrally located), a rectangular grid (as well as the original polar one) and a time dependence of the source.
The WESTIGAUSS model employed 3 different atmospheric dispersion parameter calculations. The first two WESTIGAUSS model both used a different Pasquill-Gifford parameterization. The first yielding an average snow deposition of 189,07 mg/m².d, which was much higher than the average measured snow deposition (31,83 mg/m².d). The first model also did not display a good correlation to the snow measurement or AEROPOL results. The second Pasquill-Gifford parametrization yielded a better correlation, but results were similar to the first parameterization. The third WESTIGAUSS model used the Bultynck-Malet parameterization. This yielded an average snow deposition of average snow deposition of 4,78 mg/m².d, which is very low especially compared to the measured average snow deposition (31,83 mg/m².d). However, this model showed the best correlation to the snow measurements of all the models as well as the AEROPOL results. Therefore this model was used to model the reference years 1971, 1975, 1985, 1995 and 1999. It was hypothesized that the total deposited concentration would be dependent on the total fly ash emission and therefore would decrease proportionally with a decrease in emission. Mean and maximum concentrations were predicted by the WESTIGAUSS model, this yielded the following results:

- 1971 : mean = 46,06 mg/m².d & max = 1421,73 mg/m².d;
- 1975 : mean = 9,22 mg/m².d & max = 614,45 mg/m².d;
- 1985 : mean = 23,85 mg/m².d & max = 3818,70 mg/m².d;
- 1995 : mean = 4,39 mg/m².d & max = 102,48 mg/m².d;
- 1999 : mean = 4,59 mg/m².d & max = 298,70 mg/m².d.

The year 1985 displayed a very high maximum value, which could be explained by the WESTIGAUSS tendency to overpredict maximum values. 1971, 1975 and 1995 showed a declining tendency in deposition values, which is in accordance to the AEROPOL predictions.
^{210}Pb was chosen as a reference radionuclide in accordance with the AEROPOL model. A constant activity concentration was used, namely 204 Bq/kg, in order to estimate the dose rate deposition. the WESTIGAUSS model displayed the same tendency in steady decline of deposition (with the

exception of the year 1985), results were similar in the radiological burden on the environment. As shown by the AEROPOL research the anthropogenic sources of ^{210}Pb constituted 20-28% of the natural background value (92-133 Bq/m².y) in the 1970's and 1980's. WESTIGAUSS predicted higher maximum values consistently throughout all simulations, which may be due to the Bultynck-Malet parametrization; however, this cannot be said with absolute certainty.

4. Abstract in Dutch

Het is alom geweten dat onze omgeving licht radioactief is, inclusief de atmosfeer. Bij toeval is de atmosfeer ook de ideale omgeving voor dispersie van natuurlijke of artificiële radionucliden. Volgens voorgaande studies is de olie industrie, waar 'oil shale' verbrand wordt, de grootste producent van NORM (Naturally Occurring Radioactive Materials) afval in Estland. Een geschatte 11-12 miljoen ton oil shale, hetgeen verscheidene hoeveelheden natuurlijk voorkomende radionucliden bevat, wordt jaarlijks verbrand in de Narva krachtcentrales. Dit verbrandingsproces voorziet 90% van de Estlandse elektriciteitsproductie.
Dit onderzoek focuste op het evalueren van verscheidene modellen (WESTIGAUSS, AEROPOL & IFDM) die trachtten de radionuclide concentratie rond de krachtcentrales te modeleren.
Bovenop de vliegas emissie, veroorzaakt door de verbranding van de shale oil, blijven radionucliden gehecht aan de verscheidene as fracties bij de separatiepunten en worden ze bijgevolg geëmitteerd met deze. Grond in de buurt van de krachtcentrales bevatten hogere concentraties aan ^{226}Ra en ^{210}Pb. Recente studies hebben aangetoond dat atmosferisch ^{210}Pb activiteit een grote variabiliteit vertoond in wekelijkse, seizoen afhankelijk & jaarlijkse waarden.
De verkregen resultaten van het WESTIGAUSS (We STIck to GAUSS) model, gebruikt & ontworpen door het SCK-CEN, met de resultaten van het AEROPOL model alsook een derde model namelijk het IFDM (immission frequency distribution model) werden onderling vergeleken. Alle resultaten werden ook vergeleken met sneeuw metingen genomen in Estland.
Het IFDM model voorspelde een gemiddelde sneeuw depositie van 11,63 mg/m².d terwijl de gemiddelde gemeten sneeuw depositie 31,83 mg/m².d bedroeg. Het IFDM model vertoonde alsook een slechte correlatie met de sneeuw depositie metingen, waardoor het uitgesloten werd voor verdere simulaties.
De originele WESTIGAUSS code werd succesvol uitgebreid om drie nieuwe functionaliteiten te bevatten. Namelijk de incorporatie van meerdere bronnen (en zo ook niet gecentraliseerde bronnen), een rechthoekig assenstelsel (als uitbreiding op het originele polaire stelsel) en een tijdsafhankelijkheid van de bron.
Het WESTIGAUSS model werd gebruikt om 3 verschillende atmosferische dispersie parameter berekeningen te vergelijken. De eerste 2 gebruikten de Pasquill-Gifford definitie. Het eerste model leverde een gemiddelde sneeuw depositie van 189,07 mg/m².d, hetgeen veel hoger was dan de gemeten sneeuw depositie (31,83 mg/m².d). Het eerste model toonde ook een slechte correlatie met de gemeten sneeuw depositie alsook het AEROPOL model. Het tweede model toonde een betere correlatie aan met de gemeten sneeuw depositie, maar de resultaten bleven gelijkaardig. Het derde WESTIGAUSS model gebruikte de Bultynck-Malet parametrisatie. Dit leverde een gemiddelde sneeuw depositie van 4,78 mg/m².d, hetgeen zeer laag is in vergelijk met de gemeten sneeuw depositie (31,83 mg/m².d). Dit model vertoonde wel een betere correlatie met de sneeuw metingen alsook het AEROPOL model. Vanwege deze correlatie werd dit model gekozen om de referentie jaren 1971, 1975, 1985, 1995 en 1999 te simuleren. Verondersteld werd dat de totale neergeslagen concentratie afhankelijk zou zijn van de totale vliegas emissie en daardoor proportioneel zou afnemen wanneer deze emissie daalde. Gemiddelde en maximum concentraties werden voorspeld door het WESTIGAUSS model. Deze waarden bedroegen:

- 1971 : gemiddelde = 46,06 mg/m².d & maximum = 1421,73 mg/m².d;
- 1975 : gemiddelde = 9,22 mg/m².d & maximum = 614,45 mg/m².d;
- 1985 : gemiddelde = 23,85 mg/m².d & maximum = 3818,70 mg/m².d;
- 1995 : gemiddelde = 4,39 mg/m².d & maximum = 102,48 mg/m².d;
- 1999 : gemiddelde = 4,59 mg/m².d & maximum = 298,70 mg/m².d.

Resultaten van het jaar 1985 vertoonden een zeer hoge maximum waarde, hetgeen verklaard zou kunnen worden door de tendens van het WESTIGAUSS model om maximum waarden te overschatten. Resultaten van het jaar 1971, 1975 en 1995 vertoonden een dalende tendens in depositie waarden, hetgeen in overeenstemming is met AEROPOL resultaten.

^{210}Pb werd gekozen als referentie radionuclide in overeenstemming met het AEROPOL model. Een constante activiteit concentratie werd gebruikt, namelijk 204 Bq/kg, om zo een schatting van de neergeslagen dosis te kunnen maken. Het WESTIGAUSS model vertoonde dezelfde tendens in proportionele daling in depositie (met uitzondering van het jaar 1985). Resultaten betreffende de radiologische last aan de omgeving waren gelijkend. Zoals aangetoond door het AEROPOL onderzoek bedroeg antropogeen ^{210}Pb activiteit 20-28% van de natuurlijke achtergrond activiteit (92-133 Bq/m².y) in de jaren 1970-1980. WESTIGAUSS voorspelde een hoger maximum concentratie in alle simulaties, dit zou mogelijk te wijten zijn aan de Bultynck-Malet parametrisatie. Dit kan echter niet met zekerheid besloten worden.

5. Introduction

The SCK-CEN (Studiecentrum voor kernenergie-Centre d'étude de l'énergie nucléaire), situated in Mol (Belgium), is one of the largest research institutions in Belgium. With over 700 employees dedicated to developing peaceful application of radioactivity. It's research has already yielded a long list of innovative and forward-looking applications for different sectors including the medical world, industry and the energy sector. [1] This research was issued by the 'Crisis Management and Decision Support' , which is a subdivision of the institute for environment, health and safety (EHS). [2]
Atmospheric distribution modeling is a keystone in determining the impact of air pollution on society. It is vital in determining exposure to mankind and the overall environment. In Estonia a large portion of energy production is produced by methods of consumption of fossil fuels (Coal, oil,…). This is achieved by two of the world's largest oil shale-fired power plants (PPs) which have been operational for over 40 years. Combusting oil shale emits various pollutants, such as fly ash, SO_x, NO_x, heavy metals, volatile organic compounds as well as radionuclides to the environment. [3] The radionuclides emitted include natural occurring radionuclides from the ^{238}U and ^{232}Th decay series as well as ^{40}K.
Studies have linked mortality with many pollutants, one such being nitrogen dioxide. [4] This is well documented and recognized by the WHO (World Health Organization). Therefore guidelines for maximum concentrations of several pollutants have been set. The most common premature deaths due to air pollution are, according to the WHO, ischeamic heart disease and strokes. Some other pollution related illnesses include chronic obstructive pulmonary disease (COPD), lung cancer and lower respiratory infections. [4]
It is common knowledge that our environment is slightly radioactive, this includes our atmosphere. Coincidently the atmosphere is also an ideal environment for the distribution of natural and artificial radionuclides from place to place. [5]
According to previous studies the oil shale industry is the largest producer of NORM (Naturally Occurring Radioactive Materials) waste in Estonia. With an estimated 11-12 million tons of oil shale containing various amounts of natural radionuclides which is burned annually in the Narva oil shale-fired power plants. This combustion process accounts for 90% of the Estonian electricity production. [6] Radionuclide activity concentrations have been found to increase in ash samples from the furnace towards the back end of the process. Radionuclide enrichment factors up to 4.2 were reported. [6]
One of the important radionuclides in atmospheric air is the naturally occurring radionuclide ^{210}Pb. It is a member of the ^{238}U decay chain, which is naturally present in the Earth's crust. [5] ^{210}Pb is formed in the decay chain after the alpha decay of ^{222}Rn, which is an inert gas. Since ^{222}Rn is an inert gas it is able to exhale from the soil and migrate to the atmosphere, transfer in air, and deposit to the ground, which causes a considerable amount of ^{210}Pb present in our environment. [5] ^{222}Rn is a short-lived nuclide, unlike its daughter ^{210}Pb, which has a half-life of 22,3 years. Sub-micron sized aerosol particles, such as fly ash, have been noticed to 'attract' ^{210}Pb atoms. For these reasons ^{210}Pb is a very interesting radionuclide in atmospheric dispersion studies. [5]
In this thesis there will be focused on evaluating several models to predict radionuclide concentrations around coal PPs. These models include WESTIGAUSS, AEROPOL and IFDM. There have been several studies where the population exposure to ionizing radiation as the result of nearby coal PPs is evaluated. One of these studies uses the verified, Gaussian-plume AEROPOL model. [3] In addition to fly ash emission, radionuclides found in oil shale remain attached to various ash fractions at ash separation points and are consequently emitted together with these fly ash fractions that escape the purification systems. [3] More volatile radionuclides such as ^{210}Pb and ^{210}Po can remain partially in gaseous form and leave the combustion system with flue gases. Fly ash emissions have been registered as high as 150 000 tons per year, therefore modeling the impact of these emissions is vital. [3] Due to the high temperature processes in the furnace of oil shale PPs spherical fly ash particles are created, which do not precipitate to the surface as fast. Due to the emission of these spherical fly ash particles deposition of radionuclides have been detected at a distance up to 70 km from the source. [3] The largest influence will however be found at the source location, where the highest deposited fly ash concentrations are. Soils near the PPs have been found

to contain elevated concentration of ^{226}Ra and ^{210}Pb. [3] There are 2 forms of precipitation dominant in the atmospheric dispersion of radionuclides namely dry and wet precipitation, this will be further discussed in the literature review.
Recent studies have shown that the atmospheric ^{210}Pb activity there is a high variability in weekly, seasonal and yearly values. [5]
This thesis will focus on comparing results of the WESTIGAUSS (WE STIck to GAUSS) model, used by the SCK-CEN, to the AEROPOL results as well as a third model, namely the IFDM (immission frequency distribution model). All these results will also be compared to snow measurements taken in Estonia. The WESTIGAUSS model also permits using different stability class definitions which will be explained in the section methods. After the evaluation of the different possible models the best preforming model will be used to simulate selected years. These years include 1971, 1975, 1985, 1995 and 1999. It is hypothesized that the total deposited concentration is dependent on the total fly ash emission and therefore will decrease proportionally with a decrease in emission. [3] This thesis will try to confirm this phenomena by comparing the chosen model's result to the AEROPOL results and estimate the radiological burden on the environment caused by the emission of radionuclides in the emitted fly ash.

6. Literary review

6.1. Natural Occurring Radioactive Materials (NORM)

According to the World Nuclear Association, which is an organization that represents the global nuclear industry, NORM (Natural Occurring Radioactive Materials) constitute one of the following categories. [7]

- Radioactive materials which occur naturally and where human activities increase the exposure of people to ionizing radiation;
- NORM results from activities such as burning coal, making and using fertilizers, oil and gas production;
- Uranium mining in which those involved are exposed to NORM in the uranium orebody;
- Radon exposure in homes.

Naturally occurring radionuclides are present in all minerals and raw materials. The most important radionuclides, for radioprotection purposes, are the radionuclides found in the ^{238}U and ^{232}Th series. It must be noted that most human activities involving these materials do not contribute a significant exposure to radionuclides comparatively to the background radiation. [7] However, in certain situations work activities can give a significant increase in exposure to these radionuclides. Materials giving rise to this enhanced exposure is more commonly known as NORM. [7]
The World Nuclear Association therefore defines NORM as follows: "NORM is the acronym for Naturally Occurring Radioactive Material, which potentially includes all radioactive elements found in the environment. However, the term is used more specifically for *all naturally occurring radioactive materials where human activities have increased the potential for exposure compared with the unaltered situation. Concentrations of actual radionuclides may or may not have been increased; if they have, the term Technologically-Enhanced (TENORM) may be used."* [7] Long-lived radioactive elements such as ^{238}U, ^{232}Th and ^{40}K as well as their decay products are examples of NORM. Since these parent radionuclides have such a long half time they have always been present in the earth's crust and atmosphere. [7] A different acronym, TENORM, is occasionally used to describe technologically enhanced NORM. TENORM occurs when by means of an industrial process the amount of radioactivity or concentration was increased. [7] However, more often these materials are also denoted as NORM. Some of the industries, as stated by the World Nuclear Association, known to deal with NORM issues include: [7]

- The coal industry (mining and combustion);
- The oil and gas industry (production);
- Metal mining and smelting;
- Mineral sands (rare earth minerals, titanium and zirconium);
- Fertiliser (phosphate) industry;
- Building industry;
- Recycling;
- Uranium mining.

NORM originating from the Earth's crust and mantle are either ^{238}U or ^{232}Th or decay products of these or ^{40}K. The 2 most important decay chains are the ^{238}U and ^{232}Th, which can be seen in figure 1. [7]

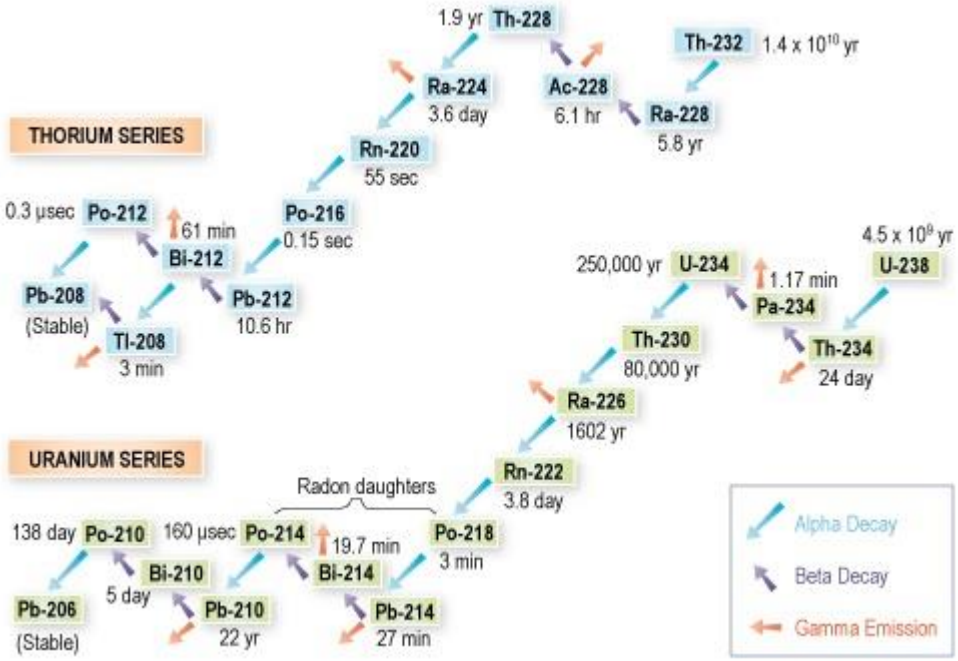

Figure 1: Thorium and Uranium decay series with corresponding decay methods [7]

NORM has been confirmed in North sea oil and gas production offshore; however, it has only been reported from one onshore production site in the United Kingdom. [8] This production site reported a high activity concentration of ^{210}Pb in metallic form. [8] However, recent studies have also found NORM activity in two further onshore sites in the East Midlands of the United Kingdom. These sites discovered elevated levels of radium. The highest ^{226}Ra and ^{228}Ra activity concentration were found in scale samples, with activities between 132 and 60 Bq/g respectively. Mean activity concentrations were found to be 86 and 40 Bq/g respectively, which is well above the national exemption levels for landfill disposal. [8] Further analysis of the scale samples showed presence of both barium and strontium. The barium-strontium concentration was then linked to the radium activity. [8] The scale and sludge samples were then dated using the ^{226}Ra/^{210}Pb method giving mean ages of 2.2 and 3.7 years. Therefore it could be concluded that these NORM deposits form in relative short periods of time, raising the issue of radioprotection and waste management. [8] These discoveries have a direct consequence when considering hydraulic fracturing of shale gas for energy production purposes. J. Garner et al. states that: “it is highly likely that other conventional oil & gas wells producing from Lower Carboniferous source rocks in the East Midlands will be similarly affected.” [4]
Normal radioactivity concentration levels of ^{238}U, ^{232}Th were found to vary between 15 Bq/kg and 27 Bq/kg and between 16 Bq/kg and 57 Bq/kg in the North Western part of India. This was reported to be less than the global average for NORM. However, elevated levels of uranium were nonetheless found in hair, nails and urine of children suffering from physical deformities, neurological and mental disorder from the Malwa region. These elevated levels were manifold higher than the reference ranges. [9]
Some studies have indicated that no hot spots of radioactivity, regarding ^{238}U, ^{235}U, ^{234}U, ^{210}Pb, ^{210}Po and ^{40}K concentrations, were observed from oil and gas industry in seawater of the northern Arabian Gulf. [10] However, this study does mention a positive and linear correlation between ^{238,234}U, ^{40}K isotopes and seawater salinity. [10]

6.2. Shell oil combustion waste

The main waste of the Estonian shale oil industry – oil shale semi-coke and ashes – are deposited in landfills. One of these, the Kohtla-Järve deposit, likely is the largest of its kind in the World. The most significant hazard to human health has been researched and concluded to be the emission of harmful landfill gases and the water contamination in local river systems. The emission of harmful gases into the atmosphere results from overheating of oil shale semi-coke because of its intensive oxidation. [11] Recent studies using a groundwater transport simulation showed that the current capping of the landfill initiated by Estiona's Ministry of the Environment has not been sufficiently substantiated. The landfill liner used is unable to contain the expansion of pollutants in ground water. [11] Since the fly ash emitted by the power plants contains radionuclides it is reasonable to assume the ashes in the landfills are also contaminated. This provides an additional hazard as according to studies the EU Landfill Directive requirements imposed on the hydraulic resistance of geological barriers cannot prevent the leakage of contaminants from this landfill. [11]

As stated before the oil shale industry is the largest producer of NORM waste in Estonia with approximately 11-12 million tons of oil shale consumption annually. [6] Activity and concentration enrichment factors were established for the ^{238}U and ^{232}Th family radionuclides using gamma spectrometry. Therefore in addition to the conventional main gaseous emissions (carbon, sulfur, nitrogen and organic compounds), oil shale combustion is also an emission source for various radionuclides. [6] These radionuclides originate since they are bound to the oil shale during the fossil fuel formation process. Even though the majority of these radionuclides remain in the precipitated ash fractions within the boiler system, a detectable amount of more volatile radionuclides are likely to be released to the atmosphere. [6] The enrichment factor for the radionuclides was defined as the radionuclide activity concentration within the ash fraction to the value in dry oil shale. [6]

6.2.1. Pulverized Firing (PF)

Pulverized firing is still the most implemented technology is the most used in the Narva Power plants. In this process fuel is pulverized into fine particles before reaching the boiler, after this pulverization the median particle size is in the range of 35-60 µm. [6] Temperatures in the PF boiler reach up to 1400 °C, which increase CO_2 emissions due to the decomposition of the carbonaceous mineral part (e.g. limestone). It is estimated that around 18 to 22% of the total CO_2 emission is due to this phenomena. [6] Temperature in the boiler's gas duct gradually decreases toward the filtration systems, which causes the flue gases emitted to the atmosphere to have a temperature in the range of 130-160 °C. [6] Two filtration systems purify the flue gas the first being an ESP (electrostatic precipitator) system and the second being a NID (novel integrated desulphurization). The ESP removes fly ash and SO_2 from flue gases. After which fly ash and flue gases are directed to the NID system reactor where they are mixed with a moist reagent. This reagent is then combined with SO_2 and precipitated through a fabric filter together with fly ash. The remaining purified flue gases are then directed to the chimney. [6] The proportion of the ash being precipitated at different stages is described in table 1.

Table 1: Ash mass flow and ash particle median size distribution in different parts of the PF system. [6]

Parameter	**Furnace**	**Superheater**	**Economizer**	**Cyclone**	**Pre-precipitator**	**ESP1**	**ESP2**	**ESP3**	**ESP4**
Ash mass flow, PF boiler, %	39,3	3,1	4,7	32,2	1,9	13,5	3,1	0,6	0,1
Median size, µm	230-270	140-180	130-170	50-60	40-50	8-12	7-10	6-8	5-6

The following figure 2 represents a schematic of these PF system including its separation systems.

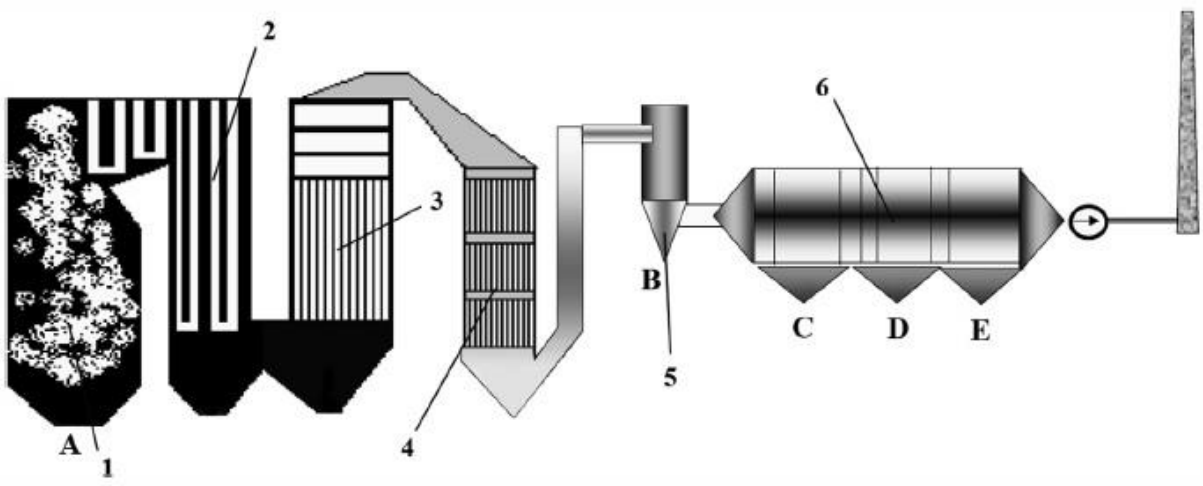

Figure 2: PF boiler in Narva Power Plants. Numbers indicate various boiler elements. 1 - furnace chamber; 2 - superheater and reheater; 3 - economizer; 4 - air preheater; 5 - cyclone; 6 - electrostatic precipitator (ESP). Letters indicate sample collection points a) bottom ash; b) cyclone ash; c) ESP1; d) ESP2; e) ESP3 [6]

Large quantities of fly ash are produced as a consequence of the oil shale composition, namely a high mineral composition and a relatively modest content of the organic part (10-65%). The oil shale burned at the Narva power plants is a mixture of extracted fuel from underground mines and from quarries. The relative quantities are varied in order to achieve the necessary and desired calorific value. [6] It has been reported that PF systems have higher (up to 4 times) atmospheric fly ash emission compared to CFB (circulating fluidized bed) boilers. [6]
Research using ICP-MS technology concluded that high temperatures cause some of the trace elements to vaporize and become emitted to the atmosphere with flue gases. [12] This causes high concentrations of toxic heavy metals in the flue gases (e.g. Pb, Zn, Mn and As with a higher concentration than 200 µg/m² each). Research in modeling why this occurs revealed that certain trace metals in the fly ash are enriched as a result of volatilization/condensation phenomena. [12] As stated before the temperature decreases along the ducts, which causes trace elements and radionuclides to combine with one another. This compound in turn condense on ash and aerosol particles, this in turn causes them to be emitted to the atmosphere with the escaping fly ash. [6] Fly ash produced by a PF system is more spherical in comparison to fly ash from the CFB systems, which means PF systems release more amounts of trace elements to the environment. [6]
Radionuclide activity concentration in fly ash emissions to the atmosphere have been shown to be dependent on the kind of solid fuel which was used. [13] This implies that radionuclide dispersion rates are dependent on fuel type, the implemented burning technology as stated before and the atmospheric conditions. [6]

6.2.2. Radionuclides in fly ash emissions

The radionuclides found in the fly ashes emitted by the Estonian power plants include the following:

- ^{238}U;
- ^{226}Ra;
- ^{210}Pb;
- ^{232}Th;
- ^{228}Th;
- ^{228}Ra;
- ^{40}K.

These include all sorts of radioactive decay including alfa decay, gamma decay,….
Following are all the decay equations including half time and decay energy:

- ${}^{238}_{92}U \rightarrow {}^{234}_{90}Th + \propto ;\ T_{\frac{1}{2}} = 4{,}47\ billion\ years\ (4{,}270\ MeV)$;
- ${}^{226}_{88}Ra \rightarrow {}^{222}_{86}Rn + \propto ;\ T_{\frac{1}{2}} = 1600\ years\ (4{,}780\ MeV)$;
- ${}^{210}_{82}Pb \rightarrow {}^{210}_{83}Bi + e^{-} ;\ T_{\frac{1}{2}} = 22{,}3\ years\ (0{,}061\ MeV)$;
- ${}^{210}_{84}Po \rightarrow {}^{206}_{82}Th + \propto ;\ T_{\frac{1}{2}} = 138{,}38\ days\ (5{,}304\ MeV)$;
- ${}^{228}_{90}Th \rightarrow {}^{224}_{88}Ra + \propto ;\ T_{\frac{1}{2}} = 1{,}913\ years\ (5{,}423\ MeV)$;
- ${}^{228}_{88}Ra \rightarrow {}^{228}_{89}Ac + e^{-};\ T_{\frac{1}{2}} = 5{,}750\ years\ (0{,}055\ MeV)$.

There are a lot of factors to take into account to estimate the harmfulness of each of these nuclides. For example, high energy waves or particles are most harmful however they might get absorbed by the air negating this. Another factor might be the chemical properties of the radionuclide, as mentioned before some nuclides can be volatile making it possible to be breathe in, circumventing our natural protective layer (the skin).

6.3. Atmospheric Dispersion Models

Empirical models have been developed to model the behavior of radionuclides in the environment. These models take into account the distribution of these radionuclides and their dilution in air, water and terrestrial ecosystems. These models are a necessity in order to determine intakes and radiation doses to people and the environment.

The concentration of a radionuclide in an environmental medium, most often air, is dependent on several variables. Some of these variables include: a source term (activity per unit of time), a dispersion term, a velocity term (e.g. wind speed),…. A very basic formula can be constructed using these inputs and can be seen in the following equation 2. [14]

$$Conc\ (per\ m^3) = \frac{Q\ (per\ s)}{u\left(\frac{m}{s}\right).\gamma(m).\ z(m)}.[DF](\text{eq. 2})\ [14]$$

Equation 1 describes a situation in which a substance is introduced at a known rate Q (per s), into a diluting medium which has a flow rate of $u\ \left(\frac{\text{m}}{\text{s}}\right)$ and wherein the area is defined by the width $\gamma(\text{m})$ and height $z(\text{m})$. DF is a dimensionless dispersion factor between 0 and 1.0. The volume of material that dilutes the pollutant is defined by the product of u and the area (γz). Equation 1 concludes that the concentration of the pollutant is directly proportional to the release rate and inversely proportional to (a) the flow of the mixing media and (b) the area through which the mixture flows. In figure 3 a simple visual representation of this basic 'box' model can be seen.

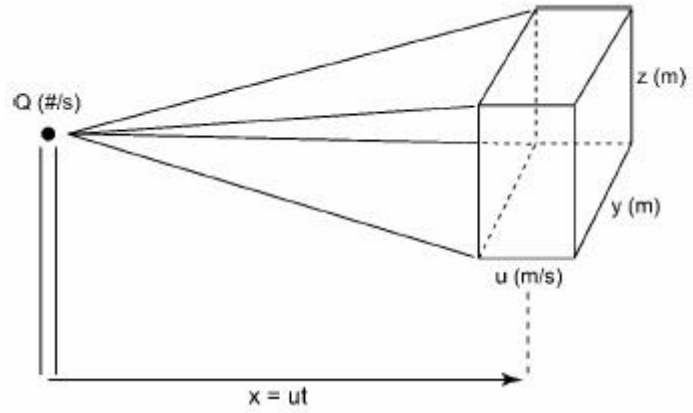

Figure 3: Simple box model for dispersion of a contaminant emitted at a rate Q into a diluent stream. [14](p. 506)

This model can be applied to several situations ranging from surface water dispersion to atmospheric dispersion. This research will focus on the latter.

In most cases the atmospheric release of a pollutant can be regarded as a point source, which emits materials at a rate of Q (per s). In some cases the value of Q may vary in time, some models take this into account however often the average Q value is used as if it were to be emitted constantly. The emitted particles enter the atmosphere where they are mixed into the atmospheric volume, which has a certain turbulence profile, that flows past the release point with a velocity u (m/s). The pollutant will be diluted in a volume of air equal to width y (m) and height z (m) multiplied by the translocation rate of air (being the air velocity u (m/s)). For a radionuclide this results in the following basic equation 3.

$$Conc\ \left(\frac{\text{Ci}}{\text{m}^3}\right) = \frac{Q\left(\frac{\text{Ci}}{\text{s}}\right)}{u(yz)}\ (eq.3)\ [14]$$

This general relationship is reasonably accurate for plumes released at a steady rate (constant Q) and confined to flow through a specific area (which limits the turbulence). [14]

Many models base their calculation on Gaussian-distributed plumes in which the atmosphere is not confined (unlike the situation of equation 3). The concentration will still be directly proportional to Q and inversely proportional to the wind speed, however some more fluctuation is observed across areal segments of the plume. For continuously emitting sources, diffusion in the downwind direction is completely dominated by the wind speed *u*; however, both the vertical and horizontal spread of the

plume increase with distance downwind. This spread is represented by the Gaussian dispersion coefficients σ_y and σ_z. A visual representation of this spread can be seen in the following figure 4. [14]

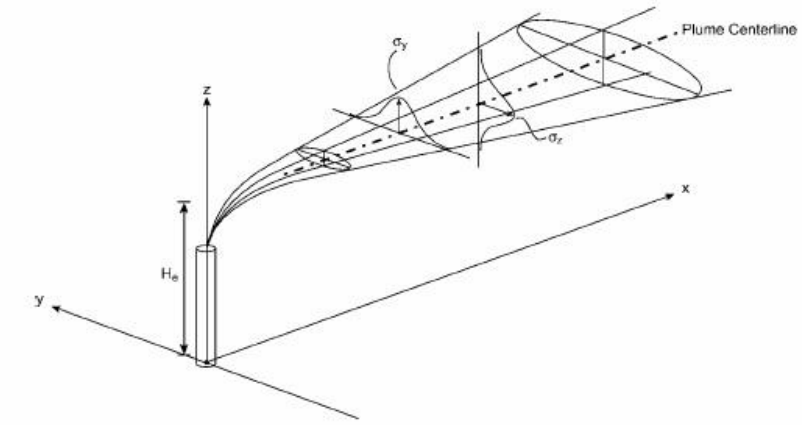

Figure 4: Atmospheric distribution of material released from a point source of height H above the ground [14](p. 508)

Taking into account this spread, represented by σ_y and σ_z, equation 3 is altered resulting in equation 4.

$$concentration\ (per\ m^3) = \frac{Q}{u.2.\pi.\sigma_y.\sigma_z}.\exp\left(-\frac{y^2}{2.\sigma^2{}_y}\right).\exp\left(-\frac{z^2}{2.\sigma^2{}_z}\right)\ (eq.4)\ [14]$$

However this equation is only suitable for 'idealized" free spaces with no barriers. In real-world applications plume reflection by the ground has to be accounted for. This is accomplished by using a 'virtual source' which also emits contaminate at a rate *Q* an equal distance, *-H*, below the ground. This results in the following equation 5. [14]

$$\chi(x,y,z,H) = \frac{Q}{u.2.\pi.\sigma_y.\sigma_z}.\exp\left(-\frac{y^2}{2.\sigma^2{}_y}\right).\left[\exp\left(-\frac{(z-H)^2}{2.\sigma^2{}_z}\right)+\exp\left(-\frac{(z+H)^2}{2.\sigma^2{}_z}\right)\right]\ (eq.5)\ [14]$$

Where χ = concentration (per m³) of the contaminant at a distance *x* downwind and at coordinates *y* = horizontal distance from the plume centerline and *z* = height above ground; *Q* = release rate of contaminants (per s); *u* = wind speed; *H* = height taking into account the real and virtual source; σ_y = horizontal dispersion coefficient (m) ; σ_z = vertical dispersion coefficient (m). [14]

There are several other modeling possibilities like Land Use Regression modelling (LUR) or Computational Fluid Dynamics modelling (CFD) however both these models are designed for very particular situations and cannot be effectively used in situations which they were not designed for. [15]

6.4. Meteorology of dispersion

In atmospheric dispersion models air is most often assumed as an ideal gas, as this is a good approximation. A volume of air is supported in place by the pressure difference between the top and bottom. This leads to the following equation 6. [16]

$$[P(z) - P(z + dz)\,].A = \rho.g.A.dz\ (eq.6)\ \ [16]$$

Where ρ is the air density within the volume and g is the acceleration of gravity. Considering air is a bad conductor and normal air movement is fairly rapid exchange in temperature is neglectable. As a consequence of above said simplifications atmospheric motions are adiabatic. Therefore the pressure change varies according to equation 7. [16]

$$T = constant\,.P^{(\gamma-1)/\gamma}\ (eq.7)\ [16]$$

Where γ is the ratio of specific heats at constant pressure and volume [16]. Solving these equations yields the following result : -d*T*/dz=*C*. Therefore we can conclude that the temperature decreases linearly with increasing altitude. This adiabatic lapse rate (*C*) usually has a value of 1°C/100m. However the atmosphere will only display this lapse rate in absence of vertical heat transfer (a well-mixed atmosphere). However atmospheric conditions fluctuate frequently, therefore the temperature distribution deviates substantial from the adiabatic. An overview of possible temperature profiles in function of altitude can be seen in figure 5. [16]

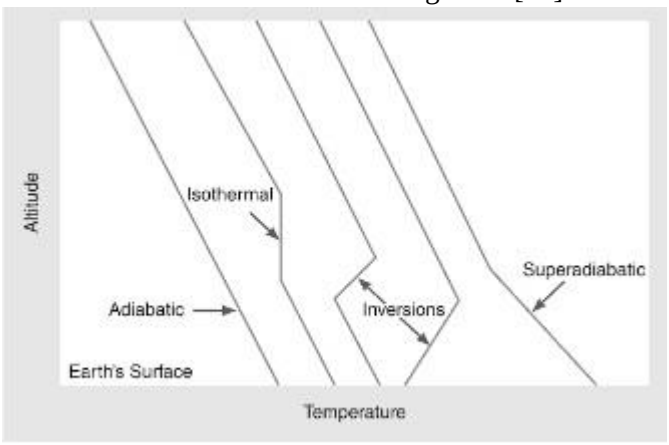

Figure 5: Possible temperature profiles in function of altitude [16] (p. 647)

The actual temperature profile is dependent on several factors. These include heating and cooling of the earth's surface, the movement of large air masses and the general surface topography [16]. Dispersion of pollutants is largely dependent on temperature profiles of the atmosphere as these influence several known influential factors of deposition (e.g. buoyance). Super adiabatic temperature conditions for example are unstable and highly favorable for the dispersing of pollutants. [16]

6.4.1. Plume Rise

The computation of plume rise is one of the basic aspects in order to achieve a correct estimation of the transport and dispersion of airborne pollutants. [17]

Whenever a plume exists a chimney it will not remain at the exit altitude (chimney height), it will either rise or fall depending on its buoyancy. [18] The plume experiences shear force at its perimeter, where momentum is transferred from the plume to the surround air meanwhile ambient air is 'sucked' into the plume. This phenomena, which is more commonly known as entrainment, is responsible for the plume diameter increase, its decrease of mean velocity and of the average temperature difference between the plume and the surround air. [17] The plume also spreads due to the buoyancy-generated turbulence, but the ambient turbulence becomes predominant with the plume traveling further from its source. [17] Complicated plume rise models are often based upon fluid dynamic equations, using the conservation of mass, momentum and energy. [17] However, in our models it was opted to use the more simplistic Briggs formula in order to entrain comparability with the AEROPOL model. Briggs (1969) developed a formula for calculating buoyancy that is applicable to all stability classes. This formula is now the standard use by most dispersion models. For the Briggs equation, first the buoyancy (F_b) has to be calculated. This is done with the following equation 8. [18]

$$F_b = g.v_s.{d_s}^2.[\Delta T/4.T_s] \ (eq.8) \text{ [18]}$$

Where g = the gravitational constant (9,82 m/s²); v_s = the stack gas exit velocity (m/s); d_s = the diameter of the stack (m); T_s = the stack gas temperature (deg. K) and ΔT = the difference between T_s and T_a (the ambient temperature). [18]

In most cases the ambient temperature is less than the exhaust gas temperature, this means that it must be determined whether the momentum of the plume or its buoyancy dominates its movement. Briggs tackles this problem by determining a crossover temperature difference. This crossover temperature, ΔT_c, is defined for $F_b \geq 55$ and for $F_b < 55$. If ΔT exceeds ΔT_c then a buoyant plume rise algorithm is used; if less, then a momentum plume rise equation must be applied. [18]

6.5. Atmospheric Stability Effects on Dispersion

As mentioned before σ_y and σ_z are defining parameters in the Gaussian plume dispersion model. These parameters are in turn governed by atmospheric properties. One of these atmospheric properties I the vertical temperature profile on the turbulence field. Classes of atmospheric stability have, therefore, been defined in terms of the temperature profile with height and variation in wind speed/ direction. As shown in figure 6a, a vertical temperature profile (steeper than the dry adiabatic lapse rate) causes a displaced parcel of the air/containment mixture to continue to rise or sink. In figure 6b a situation, in which the atmospheric temperature profile is equal to the dry adiabatic lapse rate, is displayed. In this situation the temperature of a parcel that is displaced either up or down will experience an adiabatic temperature change and will be dispersed only as far as the disturbing force moves it. This is often called a "neutral" condition, which results in a cone shaped plume. If the temperature profile is less than the dry adiabatic lapse rate, the parcel will tend to be restored to its original position as seen in figure 6c. [14]

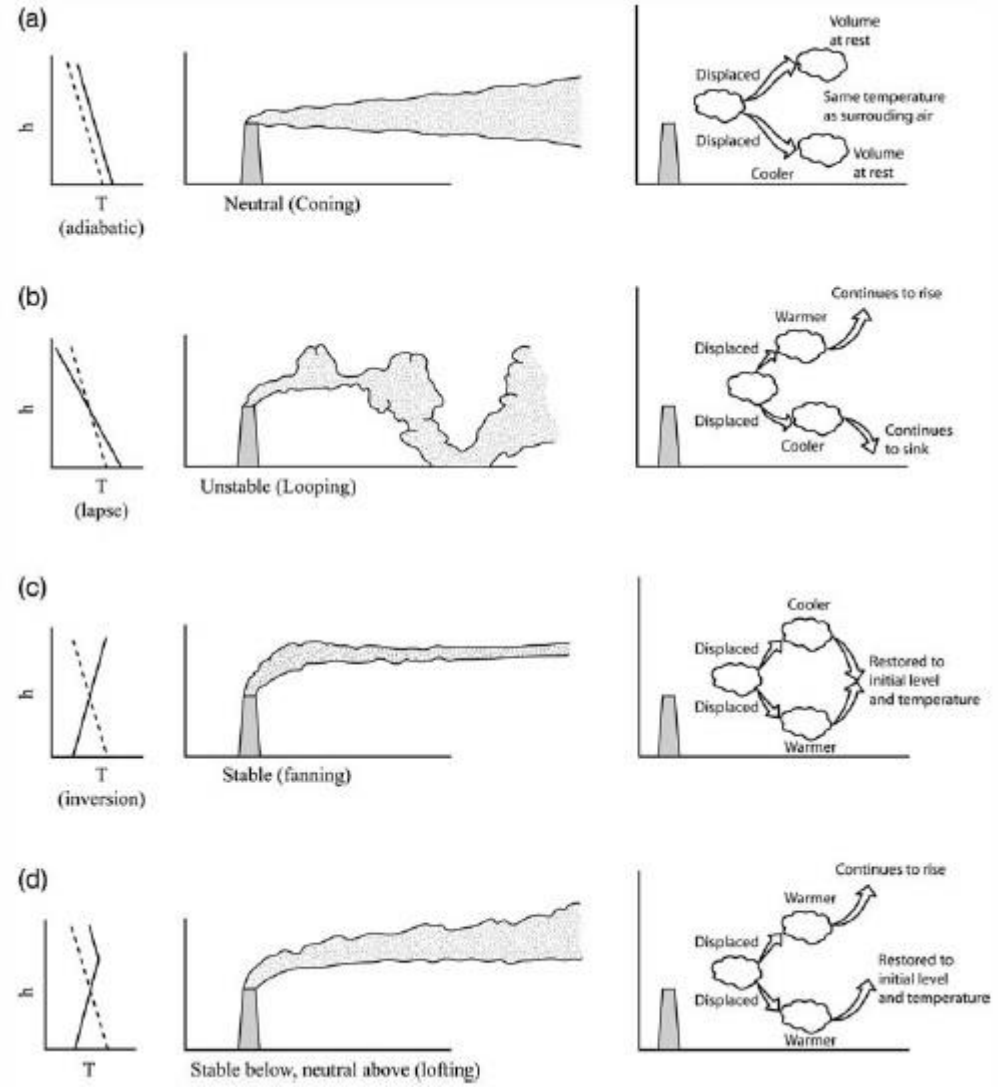

Figure 6: Effects of the vertical temperature profile on plume shape (a) lapse conditions yield looping plumes; (b) neutral conditions produce cone-shaped plumes; (c) inversion conditions result in long thin plumes; (d) inversion below/unstable above produces a condition known as lofting [14](p. 489)

In figure 6a lapse conditions occur, a parcel of the air/containment mixture in a plume is quickly displaced upward. In this movement the parcels temperature will decrease in absolute terms due to adiabatic cooling but its temperature relative to the surrounding atmosphere will be warmer making the parcel increasingly buoyant. [14] Once the parcel is displaced downward its temperature will fall more rapidly than that of the surrounding atmosphere. [14] Strong lapse conditions (which occur in super adiabatic temperature profiles) produce looping plumes that spread out over a wide area, making them inherently unstable and highly favorable for dispersal of pollutants. This phenomena can be seen in figure 6b. [14] Temperature inversions produce very stable conditions, as can be seen in figure 6c, yielding very thin plumes. When the parcel is moved upward it will be adiabatic cooled such that it will be denser than the surrounding atmosphere, therefore the parcel's movement is stopped and it returns to its original level. Any movement downward causes the parcel's temperature to increase relative to the atmosphere causing it to return to its original level. In this case it is said that the atmosphere is stable and pollutant dispersion is minimal. [14] Light winds are usually associated with stable conditions and if the wind direction is steady the plume becomes a long, meandering ribbon, however lower wind speeds do cause a higher variant wind direction. If the wind direction fluctuates significantly, the plume spreads out in the horizontal plane, this phenomena is also called fanning. This phenomena is not necessarily unwanted for the dispersion of pollutants as there is a wide horizontal spread and the plume does not touch the ground. [14] In figure 6d, a specific situation in which temperature inversion occurs beneath the plume height is displayed. This phenomena is called lofting and is the most favorable condition because effluents can disperse vertically but are kept away from the ground by a stable air layer. Thus dispersion occurs for great distances throughout large volumes of air. [14]

6.6. Atmospheric stability classes

Seven atmospheric stability classes have been defined, each of these represent the general atmospheric conditions under which they occur. Following is a list of the possible classes:

- Class A: extremely unstable conditions (bright sun, daytime)
- Class B: moderately unstable conditions (sunny, daytime)
- Class C: slightly unstable conditions (light cloudiness, daytime)
- Class D: neutral condition (overcast sky, brisk wind, day or night)
- Class E: slightly stable conditions (early evening, light winds, relatively clear sky)
- Class F: moderately stable conditions (late night, light wind, clear sky)
- Class G: very stable (predawn, very light wind, clear sky)

These classes can also be summarized in terms of wind speed and the amount of sunshine or cloudiness, as shown in table 2. This method of determining the stability class will also be used in the WESTIGAUSS model. [14]

Table 2: Atmospheric stability class as a function of wind speed and amount of solar insolation [14](p. 491)

Wind speed (m/s at 10 m)	Daytime conditions			Nighttime conditions	
	Strong sun	Moderate sun	Cloudy	>4/8 clouds	Clear sky
<2	A	A–B	B	E or F	F or G
2–3	A–B	B	C	E	F
3–5	B	B–C	C	D	E
5–6	C	C–D	D	D	D
>6	C	D	D	D	D

It is possible to have a more accurate determination of stability class if temperature is measured at different elevations and/or the standard deviation of the mean wind direction. [14]

6.6.1. Bultynck-Malet

The Bultynck-Malet parameterization is defined in equation 9 and 10.

$$\sigma_y(x; E_i) = A(E_i).x^{a(E_i)}\ (eq.9)\ [19]$$

$$\sigma_z(x; E_i) = B(E_i).x^{b(E_i)}\ (eq.10)\ [19]$$

With A,a and B,b defined by stability class using the following table 3.

Table 3: A,a and B,b determination according to stability class (Bultynck-Malet) [19]

Stability Class	**A**	**a**	**B**	**b**
E1	0,235	0,796	0,311	0,711
E2	0,297	0,796	0,382	0,711
E3	0,418	0,796	0,520	0,711
E4	0,586	0,796	0,700	0,711
E5	0,826	0,796	0,950	0,711
E6	0,946	0,796	1,321	0,711
E7	1,043	0,698	0,819	0,669

Note that the Bultynck-Malet parameterization defines the stability classes differently, therefore a conversion between both parametrization is necessary. This conversion can be seen in the following table 4.

Table 4: Pasquill-Grifford class with correspondent Bultynck-Malet class [20]

Pasquill-Grifford	**Bultynck-Malet**	**Definition**
A	E7	Extremely unstable
B	E6	Moderately unstable
C	E5	Slightly unstable
D	E3,E4	Neutral
E	E2	Slightly stable
F	E1	Stable

6.6.2. PASQUILL GIFFORD

Determining σ_y and σ_z in the Pasquill-Grifford parameterization is similar. They are calculated using the following equation 11 and 12.

$$\sigma_y(x;a) = a.x^{0,894}\ (eq.11)\ [20]$$

$$\sigma_z(x;c;d;f) = c.x^d + f\ (eq.12)\ [20]$$

With the constants a,c,d and f depending on the stability class and determined using the following table 5.

Table 5 : determination of a,c,d and f constants in Pasquill-Grifford parameterization [20]

	x ≤ 1km			***x ≥ 1 km***		
Stability class	**a**	**c**	**d**	**f**	**C**	**d**	**f**
A	213	440,8	1,941	9,27	459,7	2,094	-9,6
B	156	106,6	1,149	3,3	108,2	1,098	2,0
C	104	61	0,911	0	61	0,911	0
D	68	33,2	0,725	-1,7	44,5	0,516	-13,0
E	50,5	22,8	0,678	-1,3	55,4	0,305	-34,0
F	34	14,35	0,740	0,35	62,6	0,180	-48,6

6.7 Deposition/Depletion of Gaussian Plumes

As a plume migrates downwind they are subject to various influences. These include dispersion and dilution, both reduce the concentration of the pollutant within the plume. Large particles may settle out and pollutants within the plume may be deposited on vegetation, ground surfaces, or other objects due to physical or chemical processes. *[14]* The accumulation of contaminants on vegetation and the ground are critical since they may become entrained in food pathways and/or become a source of direct exposure from the ground surface. *[14]*

6.7.1. Dry Deposition

Dry deposition or fallout of pollutant onto vegetation and the ground surface is represented as an aerial contamination. This contamination is related to the air concentration by a constant of proportionality v_d, called the deposition velocity. This results in the following equation 13.

$$C_{A,dry}(per\ m^2) = v_d.\frac{\chi_i}{Q_i}.Q_{tot}\ (eq.13)\ [14]$$

Where Q_{tot} is the total amount of material which was released over the period that the average $\frac{\chi_i}{Q_i}$ factor is measured for a downwind sector *i*. *[14]*

The proportionality constant v_d is called the deposition velocity because it has the units of m/s. The constant have been determined experimentally by measuring the areal contamination during periods of known air concentration. Deposition velocities are also dependent on the wind velocity because the vertical profile of concentration changes with wind velocity which impacts the amount of deposition greatly. *[14]* The amount of deposition is also influenced by sorption characteristics, roughness of the underlying surface and the chemical composition of the pollutant. This variability makes even the best measured deposition velocity values have an uncertainty that can vary by an order of magnitude. *[14]* Examples of deposition velocities can be seen in table 6.

Table 6: Dry deposition velocities for selected forms of radioactive materials on soils and vegetation for several atmospheric stability conditions [14](p. 512)

Radioelement	Medium	Atm. stability	v_d (m/s)
I_2	Grass/wheat	A, B	1.4×10^{-2}
	Grass	C, D	8×10^{-3}
	Clover	C, D	$(1–2) \times 10^{-2}$
	Dry grass	E, F	1×10^{-2}
	Grass/wheat	E, F	3×10^{-3}
	Snow	–	3.4×10^{-3}
	Soil	–	3.3×10^{-3}
CH_3I	Grass	A, B	1×10^{-4}
	Grass	E, F	1×10^{-5}
SO_2	Vegetation	–	1×10^{-2} [a]
CO_2	Grass	–	2×10^{-4}
Ru	Grass	–	1×10^{-5}
	Soil	–	4×10^{-3}
Cs	Grass	–	2×10^{-3}
	Soil	–	4×10^{-4}
Zr–Nb	Soil	–	3×10^{-2}
1 μm aerosols	Grass/soil	–	1×10^{-3}
Fission products	Sagebrush	–	3×10^{-2}
Weapons fallout	Grass	–	2×10^{-3}
	Sticky ppr	–	5×10^{-3} [a]

6.7.2. Wet deposition

Pollutants can also be removed from a plume by a second process, namely precipitation. This process results in wet deposition of the plume material on vegetation, the ground surface and other exposed surfaces. Wet and dry deposition both contribute to areal contamination; however, each is regarded separately in calculations. Wet deposition calculations are fairly similar to dry deposition calculations. The biggest difference between both deposition calculations is that the constant of proportionality is a combination of the rainfall rate R and the washout ratio W_v. The washout ratio variable is dependent on the size and distribution of raindrops (or snow) and the physiochemical features of the plume. This implies that the washout ratio is a space-dependent variable; however, for practical reasons it is often assumed to be constant in respect of space. [14]
The areal contamination $C_{A,wet}$ $(per\ m^2)$ due to wet deposition is seen in equation 14.

$$C_{A,wet}(\text{per m}^2) = \frac{R.W_v.e^{-m.R}}{\lambda_e + k.R} \cdot \chi . \left[1 - e^{-(\lambda_e + k.R).t}\right] (eq.\ 14)\ [14]$$

Where χ = the contaminant concentration (usually Ci/m³) in the air above the area; R being the rainfall rate (mm/h); W_v being the volumetric washout rate; m being the plume depletion constant (h/mm); k being the vegetation washoff coefficient (mm^{-1}); λ_e being the effective removal constant (regarding radioactive and biological removal processes); and t being the duration of precipitation (h). The aerial ground concentration is also a function of dry deposition; however, this is often ignored since the wet deposition usually is much larger by orders of magnitude. [14]
In the following table, 7, some examples of the above discussed variables can be seen.

Table 7: Vegetation washoff constant k and volumetric washout factors W_v for selected radionuclides [14](p. 540)

Radionuclide	Washoff constant		Washout factor	
	Vegetation	k (mm^{-1})	Form	W_v (m^3 air/m^3 rain)
^{89}Sr, ^{90}Sr	Grass/cabbage	0.017	Fallout	5.9×10^5
^{95}Zr	Cabbage	0.022	Fallout	4.2×10^5
^{106}Ru	Lettuce	0.063	Fallout	5.6×10^6
	Cabbage	0.026	–	–
^{131}I	Grass	0.020	Fallout	3.5×10^5
	Cabbage	0.026	I_2	8.3×10^4
			Alkyl (pH 5)	4.2×10^3
^{137}Cs	Cabbage	0.02	Fallout	4.6×10^5
^{140}Ba	–	–	Fallout	4.0×10^5
^{144}Ce	Cabbage	0.025	Fallout	4.6×10^5
Particles (~1 μm)	Grass	0.063	Soluble	1.0×10^6
	Grain	0.069	Insoluble	3.0×10^5

7. Method

AEROPOL, WESTIGAUSS and the IFDM model are all Gaussian dispersion models. This means they calculate dispersion based on σ_y and σ_z parameters. However, the determination of these parameters differs between the models. WESTIGAUSS uses the Bultynck-Malet parameterization as discussed in the literary review section 6.6.1. IFDM also uses this parametrization in determining σ_y and σ_z. AEROPOL uses the alternate Pasquill-Gifford determination for both the stability classes as well as σ_y and σ_z. All 3 models use the Briggs formula to take into account plume rise. This formula can be seen in the following equation 15.

$\Delta h = 1{,}6.F^{\frac{1}{3}}.x_f^{\frac{2}{3}}.u^{-1}\ (eq.15)$ [18]

In which F = the buoyancy factor (as seen in section 6.4.3.); x_f = determined by equation 16 and u = the wind speed.

The value of x_f , with $F < 55$, is calculated as follows from equation 16.

$$x_f = 49.F^{0{,}625}\ (eq.16)$$

If $F \geq 55$ then the value of x_f is calculated using the following equation 17.

$$x_f = 119.F^{0{,}4}\ (eq.17)$$

These models were used to model winter deposition in mg/m².d for the year 1999. This data was then compared to taken snow measurements to determine the accuracy of each model.

In order to be able to make an estimating of the radiological burden on the environment the radionuclide activity concentration in the emitted fly ash has to be known. This data was obtained from previous studies. However, some assumptions has to be made to estimate the radionuclide content in the escaping fly ash due to changes in the power plants' technological set-up. [3] Since previous studies had shown a strong positive correlation between radionuclide (Bq/kg) and its stable isotope (mg/kg) concentrations, it was possible to extrapolate the radionuclide concentration from the microelement concentrations. [3] This resulted in the values seen in table 8.

Table 8: Radionuclide activity concentration (Bq/kg) used in modelling input. [3]

Combustion boiler	**^{238}U**	**^{236}Ra**	**^{210}Pb**	**^{210}Po**	**^{232}Th(^{228}Th)**	**^{228}Ra**	**^{40}K**
PF with ESP	96	105	204	204	51	51	3800

These values were used to estimate the radiological impact on the environment.

7.1. IFDM

The IFDM model uses the following equation 18 to calculate deposited concentration.

$$C(x,y,z) = \frac{10^6.Q_0}{3600.2.\pi.\sigma_y.\sigma_z.u_{he}}.e^{-\frac{y^2}{2.\sigma^2 y}}.\left[e^{-\frac{(z-h_e)^2}{2.\sigma^2 z}} + e^{-\frac{(z+h_e)^2}{2.\sigma^2 z}}\right]\ (eq.18)$$ [21]

Where C = mass concentration (mg/m³) at a certain location (x,y,z); Q_0 = the source concentration; σ_y and σ_z the horizontal and vertical dispersion parameters respectively; h_e = the effective source height in meters and u_{he} = the wind speed extrapolated to the effective source height. [21]

The effective source height, h_e, is calculated as follows $h_e = h_g + \Delta h\ (eq.19)$. In this equation h_g signifies the geometric source height or the release point of the plume and Δh the plume rise as a consequence of , which is calculated using the Briggs formula.

It is important to note that in the IFDM manual they do not recommend using this model for calculations further away than 20 kilometers from the source as the values become unreliable. [21]

The IFDM input parameters were the following:

- Dry deposition velocity, v_d = 0,006 m/s;
- Wet deposition velocity, $\lambda = 9{,}18.10^{-5}$ m/s;

- Snow deposition velocity, λ = 0,0023 m/s;
- Source coordinates;
- Source geometric dimensions (height,…);
- Gas exit velocity, v_s.

The first source was defined at x = 722,35 (km); y = 6577,0 (km); H = 200 (m); D = 8,0 (m); T = 200 (°C); R (= v_s) = 1229,0 (N.m³/s); Q = 1133,762 g/s.

The exit velocity, v_s, was provided in the unit m/s, measured at the exit of the chimney. However, IFDM needs a normalized value in the unit N.m³/s. This value was calculated using the following method.

$$P.V = n.R.T \rightarrow V = \frac{n.R.T}{P} \rightarrow \dot{V} = \frac{\dot{n}.R.T}{P} \quad (eq.20)$$

In the above equation 20, the volume flow rate can now be compared in normalized conditions against the measured ones. Since the measurements were taken at the chimney exit the pressure, P, is the same atmospheric pressure as in the normalized value. N (amount of moles) are also the same as they are independent from temperature and pressure. However, R (gas constant) can change in function of temperature, this has been neglected as the difference is minimal and would over complicate the calculations. We can now calculate the ratio $\frac{\dot{V}_1}{\dot{V}_2}$ which is completely dependent on the temperature difference. For the first source this ratio becomes $\frac{473{,}15\ K}{273{,}15\ K} = 1{,}73$. We also know the exit velocity, v_s, for V_1. With this data we can calculate V_1 as follows from equation 21.

$$\dot{V}_1 = v_s.A\ (eq.21)$$

Applying this to the first source data yields that $\dot{V}_1 = 42{,}3\frac{m}{s}.\pi.4^2 = 2126{,}23\ N.m^3/s$. From the ratio $\frac{\dot{V}_1}{\dot{V}_2}$ we can now determine $\dot{V}_2$ as, $\dot{V}_2 = \frac{\dot{V}_1}{1{,}73}$. This yields that $\dot{V}_2 = 1229{,}03\ N.m^3/s$. These calculations were also executed for source 2 and 3 and will therefore be excluded from this.

The second source was defined at x = 734,13 (km); y = 6586,6 (km); H = 180 (m); D = 7,0 (m); T = 140 (°C); R (= v_s) = 603,14 (N.m³/s); Q = 260,7 g/s.

The third source was defined at x = 734,47 (km); y = 6586,6 (km); H = 150 (m); D = 7,0 (m); T = 180 (°C); R (= v_s) = 603,14 (N.m³/s); Q = 521,3 g/s.

7.2. WESTIGAUSS

WESTIGAUSS is, as stated before, an atmospheric dispersion code. It was designed to the specifics of the MYRRHA (Multi-purpose hYbrid Research Rector for High-tech Applications) reactor. WESTIGAUSS employs a tested Gaussian plume model using dispersion parameterization designed for the local environment at the SCK-CEN. These dispersion parameters were established by extensive experiments in which controlled released from the weather mast on site were measured. [22]
Some of the main characteristics of the code include:

- A Cartesian grid for air concentration, deposition and dose calculations with tunable dimensions and spacing;
- Dry and wet deposition, separately for aerosols and Iodine isotopes (Sohier, 2002);
- Doses from inhalation, ground shine and immersion;
- Simplified treatment of terrain features;
- Briggs formulae for the plume rise (Briggs, 1965 and 1971);
- Reflections from the ground and the inversion layer.

WESTIGAUSS is a FORTRAN 77 based program using input ASCII text files and outputting these as well. [22]
The code was validated with the use of the IFDM program, by using a full year of hourly weather data on a 50 by 50 km grid. In this validation study the calculated dilution factors were within a few per cent. The same deviation was found in shorter releases and on smaller grid sizes. [22]
In order to compare the program to AEROPOL data several changes were made to the code. These included integration of multiple sources, a different wet deposition parameter and an alteration for non-centered sources. Several methods for calculating the dispersion parameters were also implemented to review their impact on the deposition. This will be explored further in the section results subsection 8.2.

The original WESTIGAUSS code calculations deposition with a centered source. However, this is not the case in the AEROPOL code. In order to be able to compare both codes an alteration to the WESTIGAUSS code had to be done. This was achieved by transposing the source to the center,

transposing according to the wind direction and calculating as if the source was centered. The following figure 7 is a visual representation of this process.

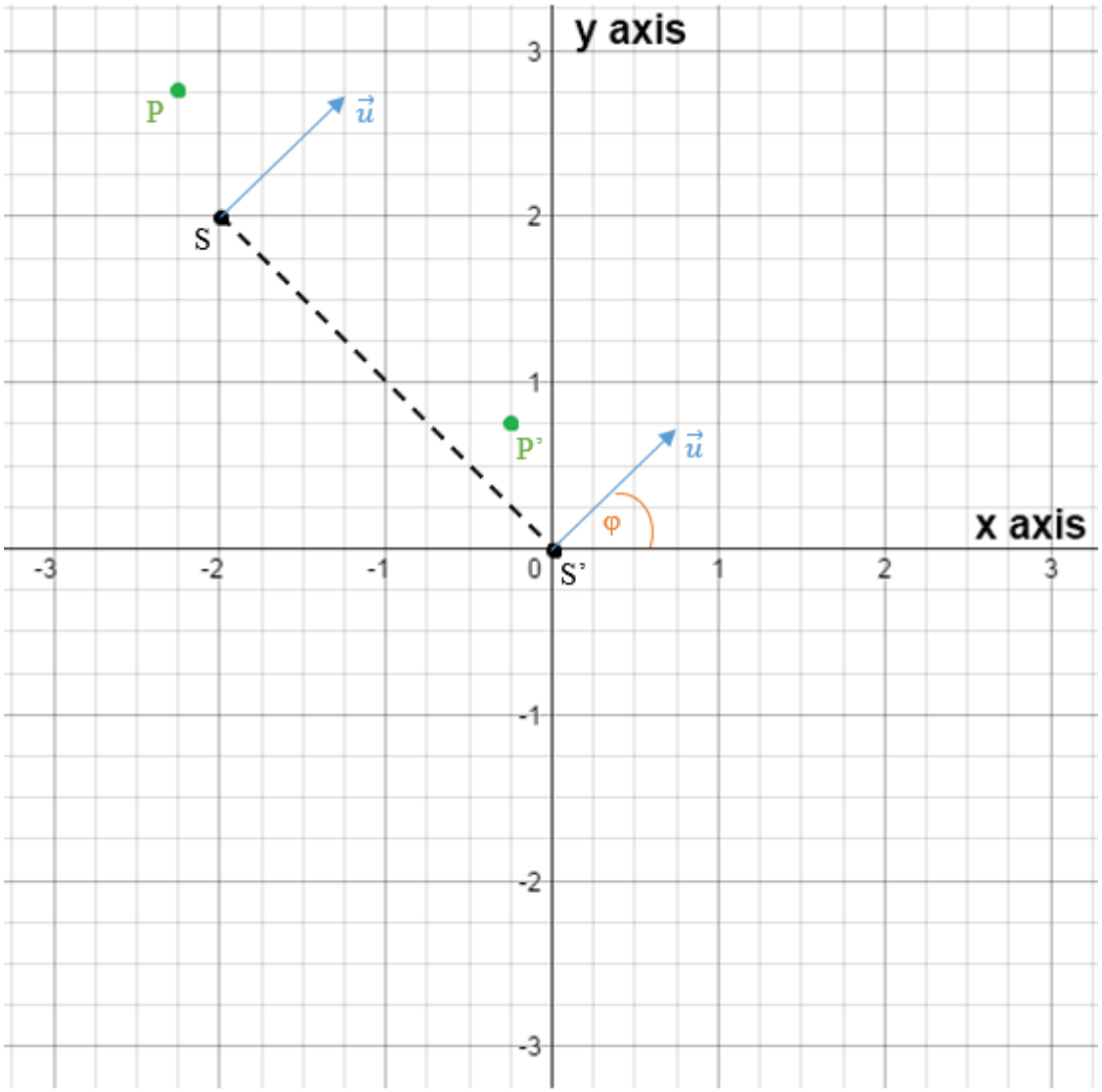

Figure 7: Transformation of a non-centered source to a centered source for calculation purposes

In figure 7, the point S is defined as the spatial coordinates of the source, being x_s and y_s. The point P is the point where the concentration has to be calculated, being x_p and y_p. In order to center the source a transformation has to be applied, this is achieved by transposing the original coordinates, centering around the source, to the axis origins. The following formulas, equation 22 and 23, were used to achieve this.

S'

$$\begin{cases} \Delta x = x - x_s \ (eq.22) \\ \Delta y = y - y_s \ (eq.23) \end{cases}$$

After this transformation was applied a second transformation was included. This involved rotation in order to match the wind vector, $\vec{u}$, with the x-axis, this to eliminate the need of a unit vector in the calculations. This simplified the code and also sped up the process speed. The rotation was achieved using the following equations 24 and 25.

$$\begin{cases} x' = \Delta x.cos\varphi + \Delta y \,.\sin\varphi \ (eq.24) \\ y' = -\Delta x.sin\varphi + \Delta y.cos\varphi \ (eq.25) \end{cases}$$

It is important to note that while the point of interest, P, was also transformed using the above explained method, its relative position to the source, S, remained unchanged. Since the deposition

value is only based upon the relative position to the source, this transformation will not change the results but merely simplify the calculation method.

7.2.1. WESTIGAUSS Pasquill-Gifford (WGPG)

Two version of the WESTIGAUSS code with Pasquill-Gifford parametrization were developed. One uses the parametrization as defined in section 6.6.2. For reasons that will be discussed in the section results subsection 8.2 another definition of the Pasquill-Gifford parametrization was used in the second version.

7.2.1.1. WGPG1

In this version the parametrization as defined in section 6.6.2 was used.

7.2.1.2. WGPG2

In the second version a different empirical formula for the definition of σ_y and σ_z was used. The formula used for the definition of these can be seen in equation 26.

$$\sigma_{y,z} = a.x^{b+c.\ln(x)} \ (eq.26) \text{ [23]}$$

In this formula *a*, *b* and *c* are defined by the least square method. This yielded the following results. Table 9 shows the results for the least square method coefficients matching the σ_y curves. Table 10 shows the results for the least square method coefficients matching the σ_z curves.

Table 9: Least square coefficients a,b and c for the Pasquill-Gifford σ_y curves [23]

Stability	***a***	***b***	***c***
A	209,6	0,8804	-0,006902
B	154,7	0,8932	-0,006271
C	103,3	0,9112	-0,004845
D	68,28	0,9112	-0,004845
E	51,05	0,9112	-0,004845
F	33,96	0,9112	-0,004845

Table 10: Least square coefficients a,b and c for the Pasquill-Gifford σ_z curves [23]

Stability Class	***a***	***b***	***c***
A	417,9	2,058	0,2499
B	109,8	1,064	0,01163
C	61,14	0,9147	0,0
D	30,38	0,7309	-0,03200
E	21,14	0,6802	-0,04522
F	13,72	0,6584	-0,05367

7.2.2. WESTIGAUSS Bultynck-Malet

The Bultynck-Malet version of the WESTIGAUSS code (WGBM) uses the definition of σ_y and σ_z as defined in section 6.6.1.

8. Results & Discussion

8.1 IFDM

The IFDM model yielded the following results.

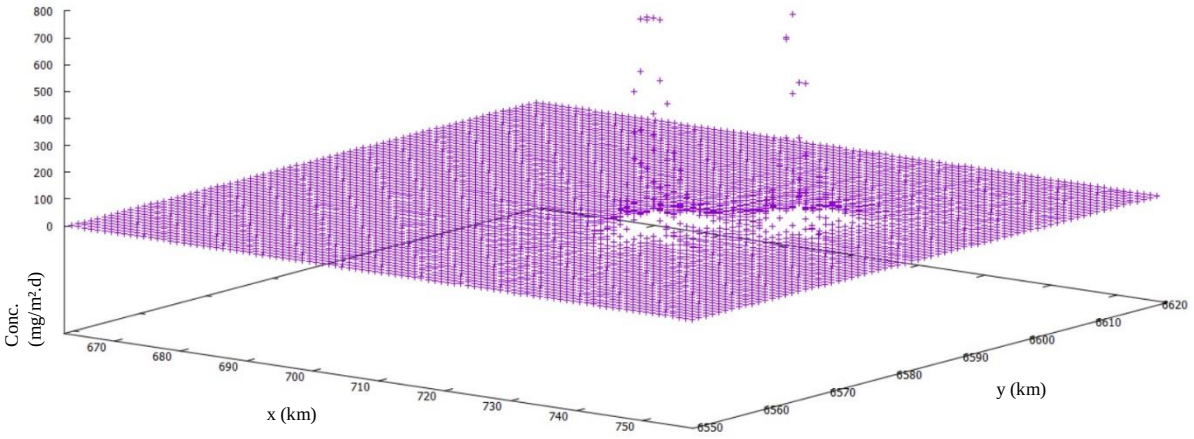

Figure 8: IFDM modeling results for the 1999 winter period (6/1/199 till 13/3/1999) in mg/m².d

Comparing the IFDM results for snow deposition to the measured ones yielded the following results (figure 9).

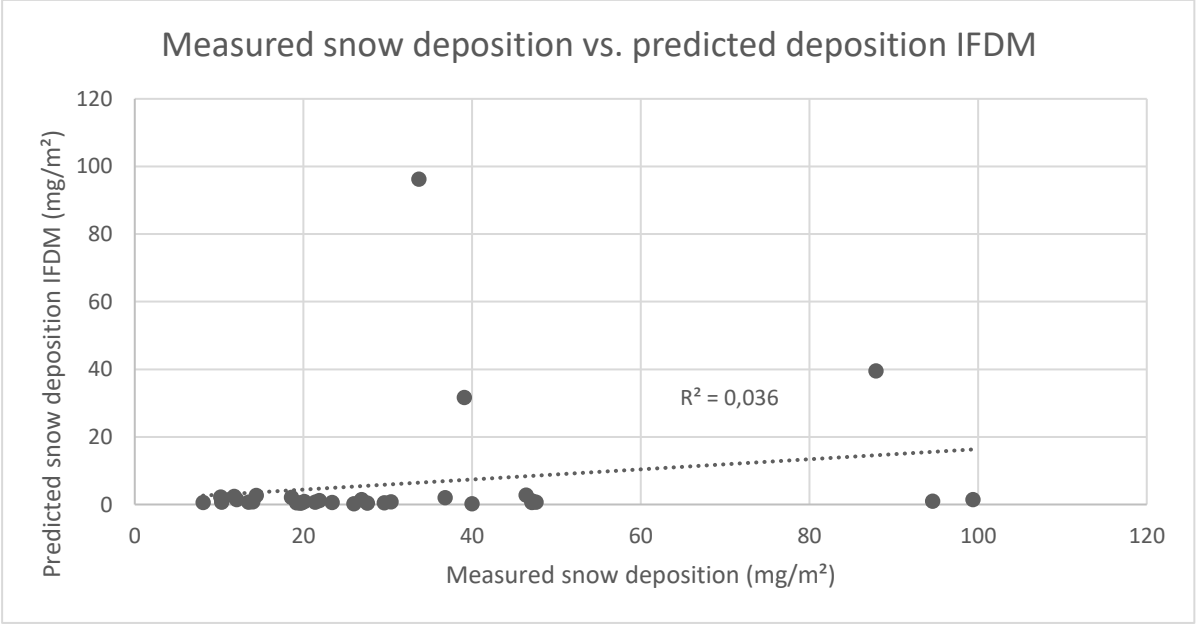

Figure 9: measured snow deposition vs. predicted deposition IFDM

IFDM predicts an average snow deposition of 11,63 mg/m².d while the average measured snow deposition is 31,83 mg/m².d. From figure 9 it is also clear that the correlation between the model and snow measurements is very low. However, when comparing dry deposition values only the IFDM model preformed fairly good, preforming with an average relative deviation to the average of 60%. This could be due to the fact that IFDM does not calculate λ based upon rain measurements but treats it as an absolute value, which is not the case in the other models. Since the IFDM model preformed badly in total deposition values it was disregarded as an option compared to the WGBM and WGPG models. This bad performance might be due to the wide array of limitations this version of the program has, including a set emission value, set wet deposition factor and many others. All these factors combined impacted the model's performance too much to be representative of this specific case.

8.2 WESTIGAUSS Pasquill-Gifford

8.2.1. WGPG1

The first parameterization as described in section 6.6.2. yielded the following results.

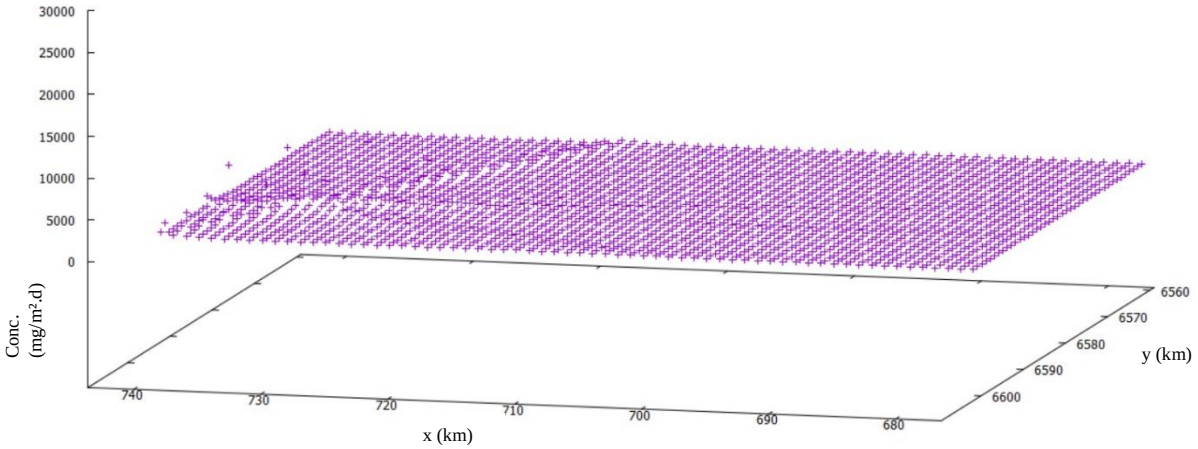

Figure 10: WGPG1 modeling results for the 1999 winter period (6/1/199 till 13/3/1999) in mg/m².d

In the above figure 10 it can be seen that the WGPG1 model predicts very high values, which is not in accordance with the AEROPOL model. Because of these high values dispersion in the lower values cannot be visually seen, therefore another plot was constructed with a set maximum value, this can be seen in figure 11.

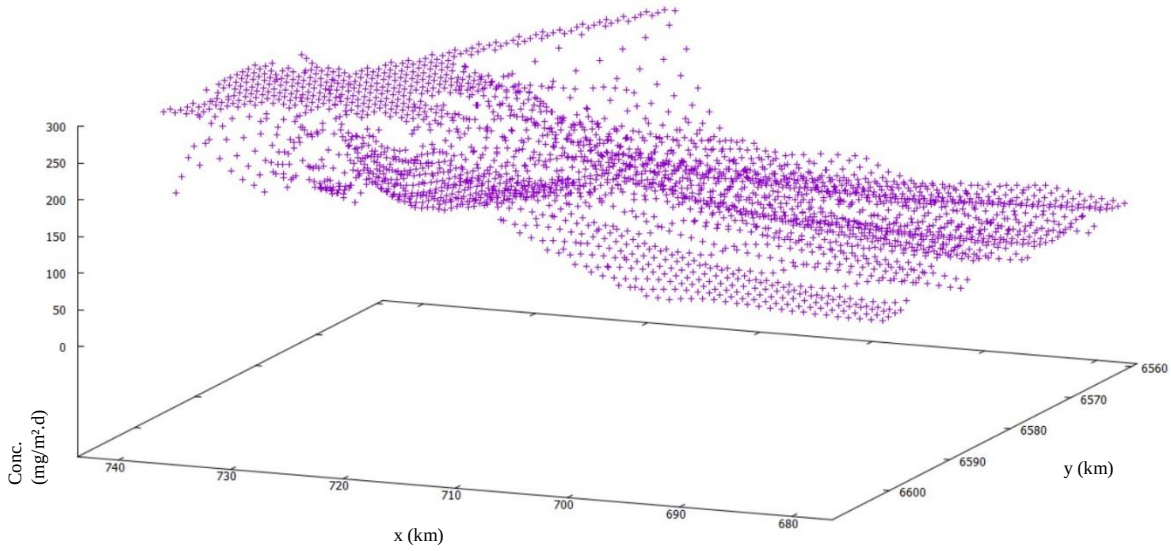

Figure 11: WGPG1 modeling results for the 1999 winter period (6/1/199 till 13/3/1999) in mg/m².d with a set maximum value (300 mg/m².d)

With a set maximum value dispersion in the lower values can be visually recognized. Examination of the dispersion parameters (σ_y and σ_z) showed expected values. However, when the input parameter for the calculation of the dispersion parameters was changed to the unit of meters instead of kilometers the following result was achieved (figure 12).

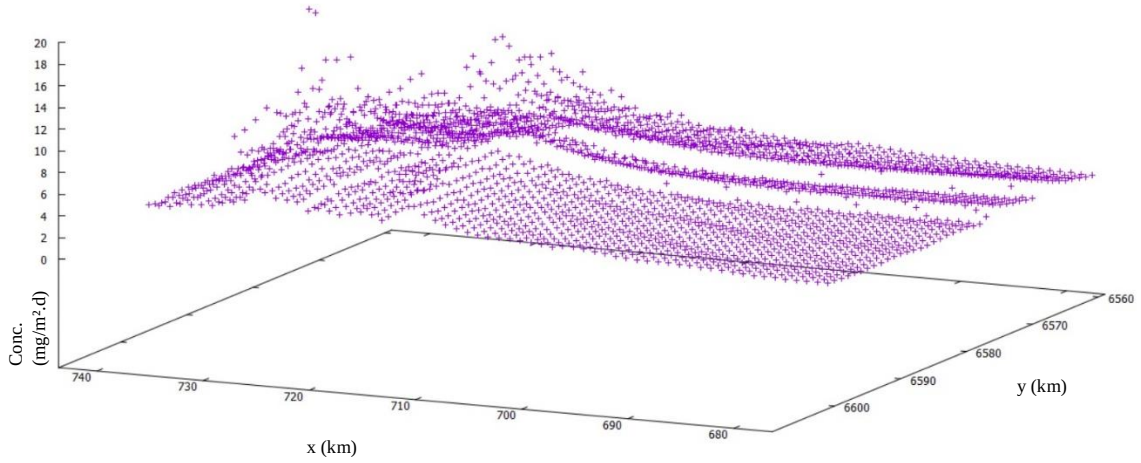

Figure 12: WGPG1 modeling results for the 1999 winter period (6/1/199 till 13/3/1999) in mg/m².d with dispersion parameters calculated using x in meters

Visually this resembles a more realistic dispersion model; however, when reviewing the dispersion parameter values it was concluded that this was impossible as the values reached values of upwards a million while it's expected values do not exceed 10^4 and 3.10^3 for σ_y and σ_z respectively in the Pasquill-Gifford definition of these parameters. This can be seen in the following figure 13.

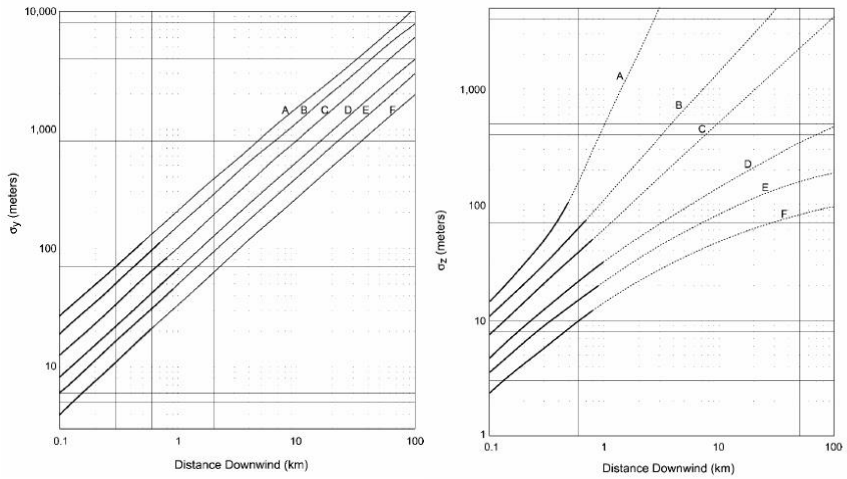

Figure 13: σ_y and σ_z values in function of downwind distance in km in the Pasquill-Gifford definition [14](p. 492-493)

Comparing the WGPG1 model (with *x* in km) yielded the following result.

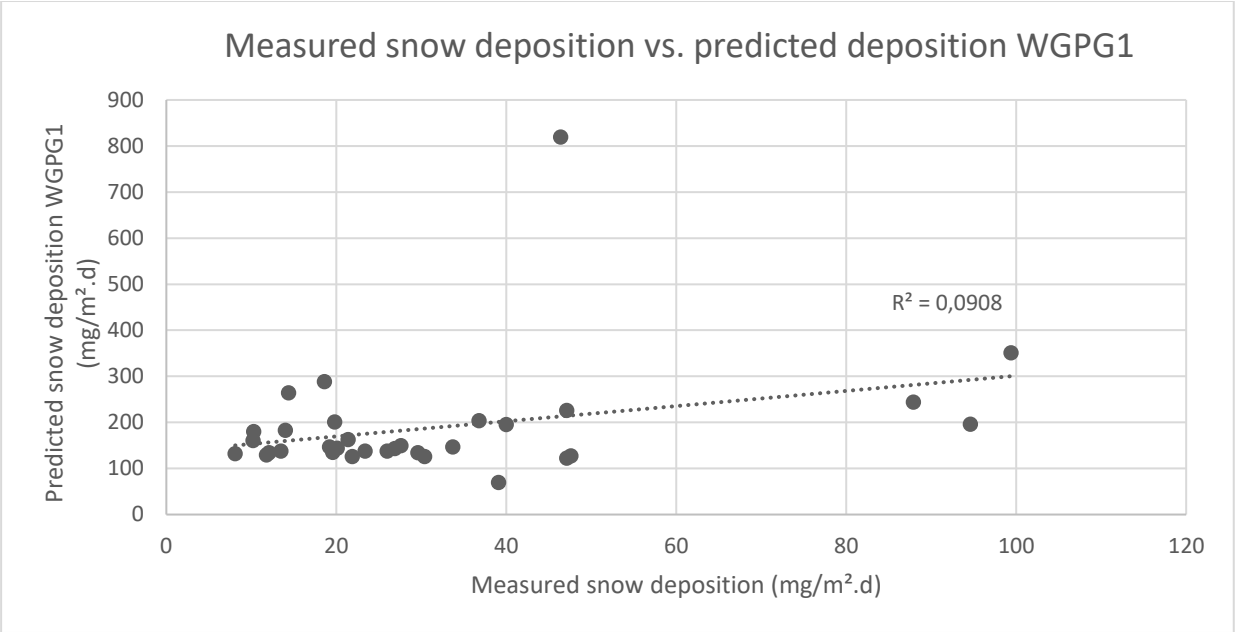

Figure 14: measured snow deposition vs. predicted deposition WGPG1

From figure 14 it is clear that the predicted snow deposition is much higher than the measured deposition. WGPG1 predicts an average snow deposition of 189,07 mg/m².d, which is much higher than the average measured snow deposition, which was 31,83 mg/m².d. There also does not seem to be a good correlation between the results from WGPG1 to the AEROPOL results. This is of course highly influenced by the very high values predicted by WGPG1, but even with these excluded the correlation is practically nonexistent.

8.2.2. WGPG2

Since AEROPOL uses the Pasquill-Gifford parameterization such high deviations as in WGPG1 were unexpected. Therefore a different definition of WGPG2 was used in order to compare both methods. This yielded the following results.

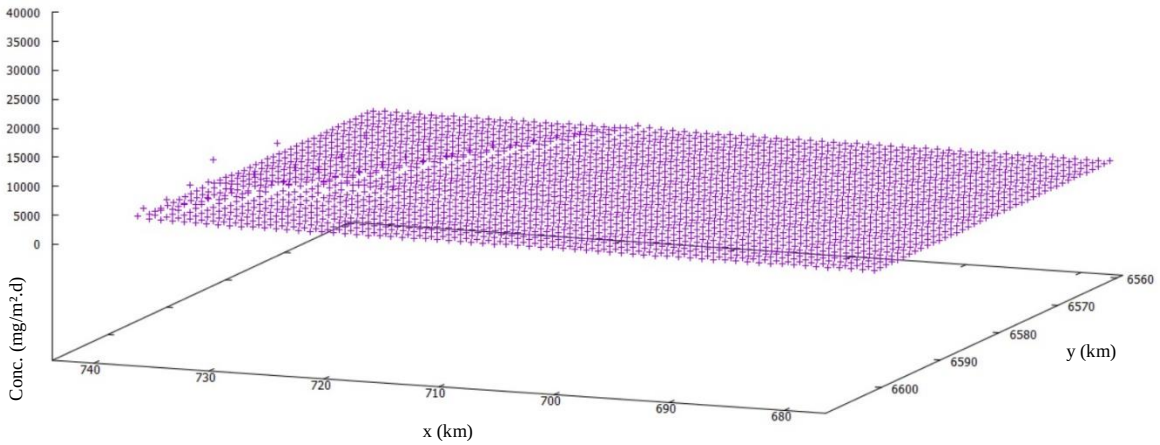

Figure 15: WGPG2 modeling results for the 1999 winter period (6/1/199 till 13/3/1999) in mg/m².d

As expected WGPG2 yielded very similar results to WGPG1.
Comparing WGPG2 to the snow measurements yielded the following results.

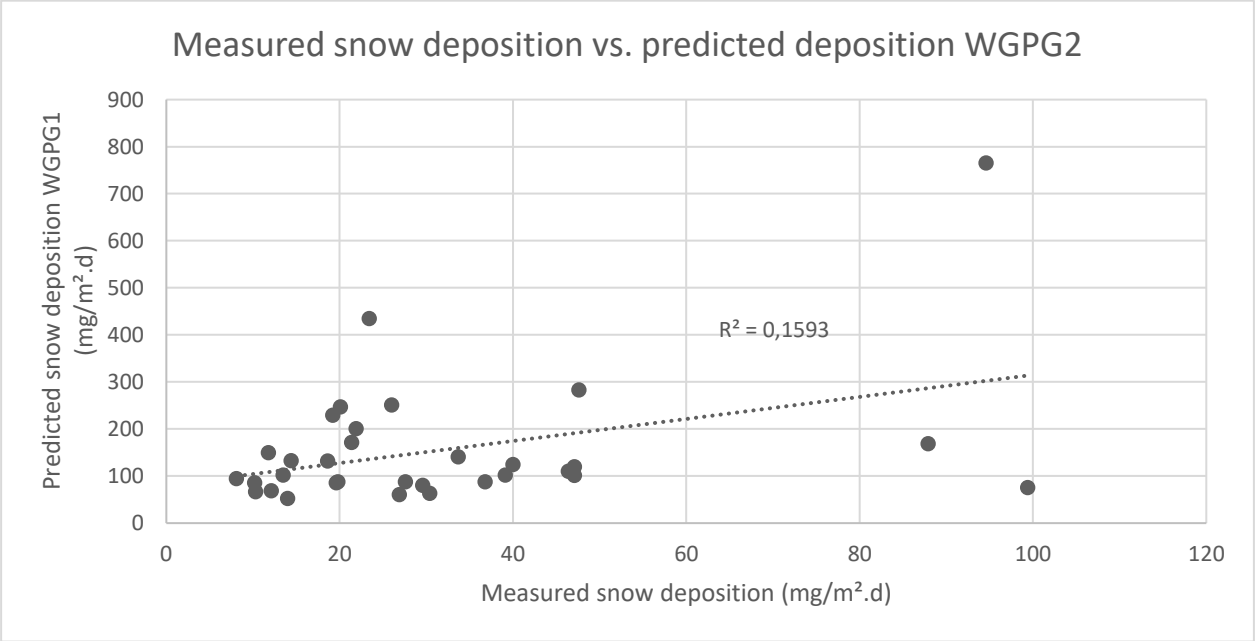

Figure 16: measured snow deposition vs. predicted deposition WGPG2

The same conclusions as for WGPG1 are still in effect for WGPG2; however, WGPG2 does seem to have a higher correlation with the snow measurements than WGPG1. This indicated that WGPG2 preforms better in lower concentration deposition calculations than WGPG1.
It is important to note that WGPG2 does not show the same tendency to alter its form when calculating the dispersion parameters with x in meters.

8.3 WESTIGAUSS Bultynck-Malet

The Bultynck-Malet parameterization was developed on site by the SCK-CEN. It was designed specifically for this site and use outside of it has not yet been researched. In the following figure 17 the result for the 1999 winter period can be seen.

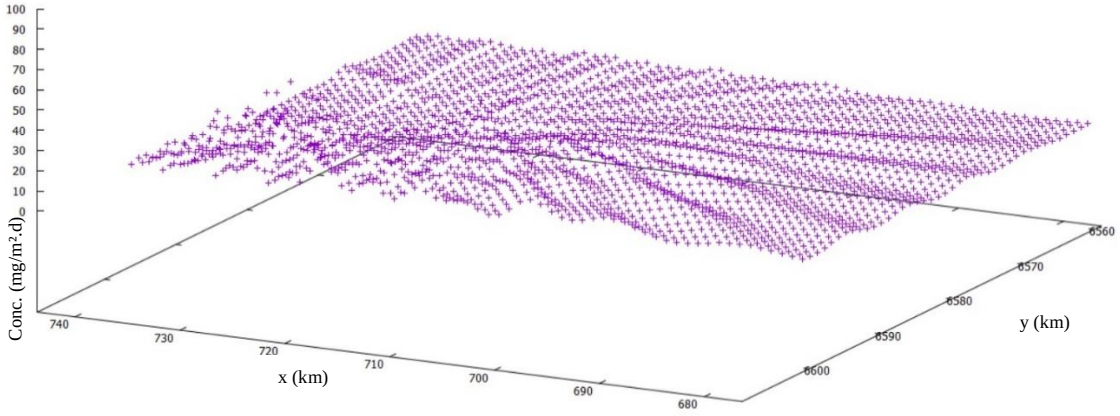

Figure 17: WGBM modeling results for the 1999 winter period (6/1/199 till 13/3/1999) in mg/m².d

In addition the WGBM model was also plotted using the Surfer 15 program this can be seen in the following figure 18.

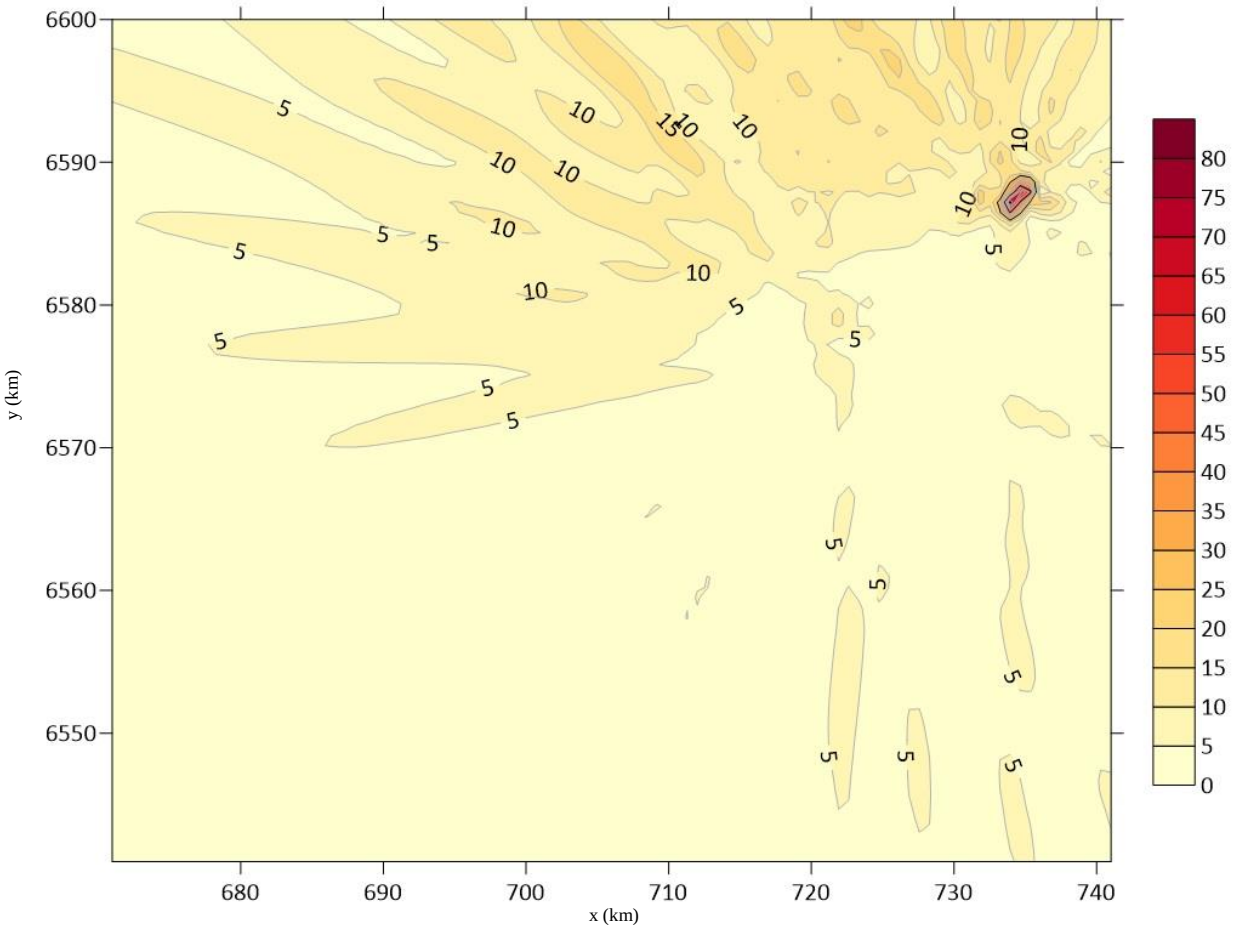

Figure 18: WGBM contour plot ('Heatmap') for the 1999 winter period modeling results (6/1/199 till 13/3/1999) in mg/m².d

WGBM does not predict the same high value outliers that both WGPG models predicted. It instead seems to 'spread' the concentration more and predicts more fluctuations in every direct than the WGPG models. This resembles the AEROPOL predictions more. Statistical analysis of the WGBM

results yields a mean value of 4,93 mg/m².d which is very low. This can be explained due to the fact that the results have a very low standard deviation meaning the data tends to be close together. This can also be seen in the percentiles in which the data is divided, namely 90% of the data (results) is situated below 10,11 mg/m².d. While only 1% of the data is situated above 17,62 mg/m².d, indicating that the overall spread of the emitted fly ash is high and the highest dose is concentrated in one particular area, namely the source point(s).
WGBM displays a much better correlation with the AEROPOL; however, WGBM does predict significantly lower results as will be discussed further in section 8.4.
Comparing WGBM to the snow measurements yielded the following results.

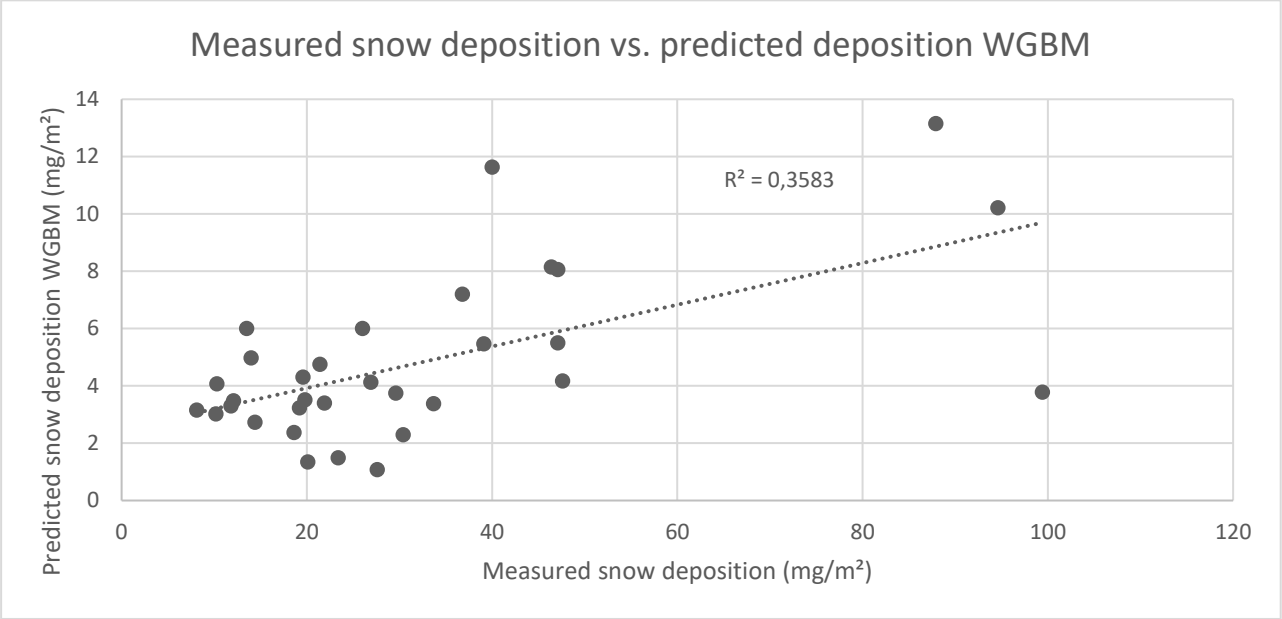

Figure 19: measured snow deposition vs. predicted deposition WGBM

WGBM's snow predictions are generally much lower (near to a factor of 10) than the measured snow depositions. However, the correlation between the predictions and the measurements is significantly higher than in the other models (excluding AEROPOL) as seen in figure 19. WGBM predicts an average snow deposition of 4,78 mg/m².d, which is very low especially compared to the measured average snow deposition (31,83 mg/m².d). Research has shown that the constant λ for wet deposition due to snow fluctuates significantly depending on which radionuclide is used. [24] [25] However, since the same λ coefficient for snow deposition was used as in the AEROPOL model this should not be the cause of the deviation especially since the AEROPOL model does not display this same behavior.

8.3.1. Deposition throughout the years

In the above section it is established that the Bultynck-Malet version of the WESTIGAUSS code preforms best in accordance to both the snow measurement as well as the AEROPOL model. The reference years 1971, 1975, 1985, 1995 and 1999 were therefore modeled using the WESTIGAUSS Bultynck-Malet version. This yielded the following results.

8.3.1.1. 1971

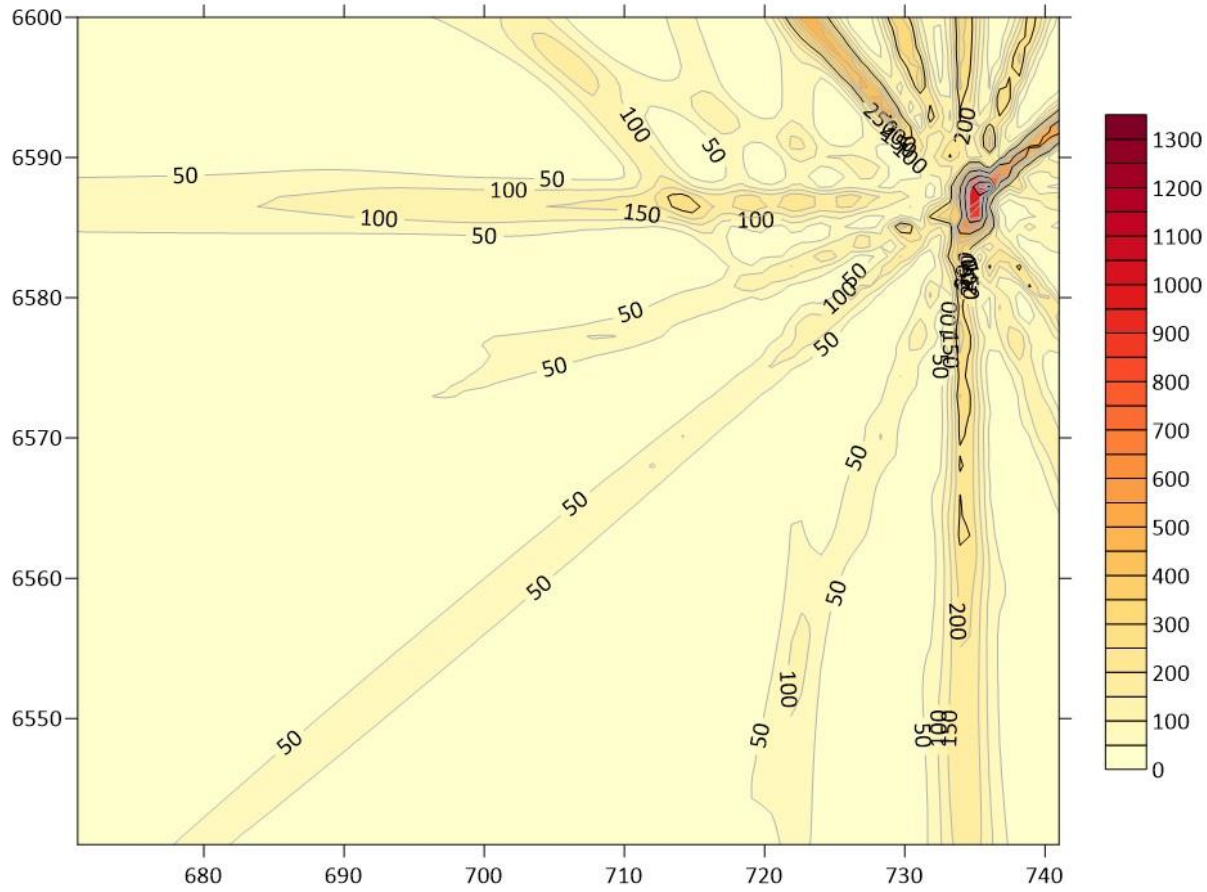

Figure 20: WGBM contour plot ('Heatmap') for the year 1971 modeling results in mg/m².d

Modeling results for the year 1971 can be seen in the above figure 20. Visually can be seen that the maximum concentration is predicted at the source point(s). One of these source points is more profoundly outspoken because of the higher emitted fly ash value (near to double) which directly correlates with the deposition. From the center cone shaped plumes which are fairly narrow take off. Statistical evaluation of the deposition values yielded a mean value of 46,06 mg/m².d. This is impacted greatly by the extremes predicted at the source points as can be seen from the 50%-tile value of 18,42 mg/m².d, which indicates that half the dataset is situated below 18,42. This is even more apparent when comparing the mean value to the median value of 18,43 mg/m².d which indicates even further that the mean is heavily impacted by the predicted extremes. The predicted maximum is 1421,73 mg/m².d.

From the previous research by (Vaasma et al, [3]) we can now calculate the dose rate due to the deposited fly ash for any of the radionuclides in table 8. For ^{210}Pb this would yield an average dose rate of $46{,}06\,\frac{mg}{m^2.d}\,.\frac{204}{10^3}\frac{mBq}{mg} = 9{,}40\,\frac{mBq}{m^2.d}$ and a maximum dose rate of $1421{,}73\,\frac{mg}{m^2.d}\,.\frac{204}{10^3}\frac{mBq}{mg} = 290{,}03\,\frac{mBq}{m^2.d}$.

8.3.1.2. 1975

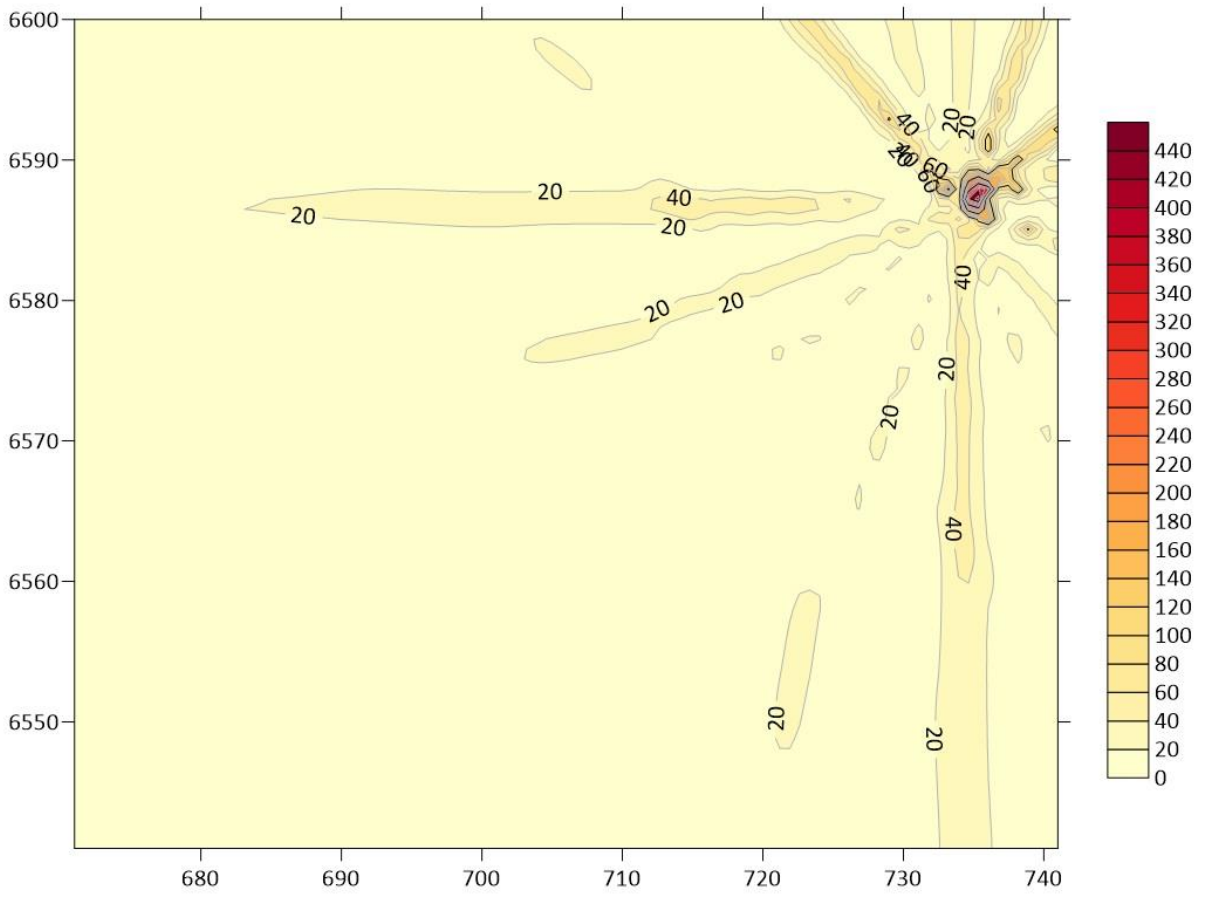

Figure 21: WGBM contour plot ('Heatmap') for the year 1975 modeling results in mg/m².d

In the above figure, 21, modeling results can be seen for the year 1975. Visually the same tendencies as in the year 1971 continue, namely a pronounced maximum at the source point(s) as well as the cone shaped narrow plumes; however, this last phenomena is less profound in the 1975 results. Statistical analysis yields the following defining parameters. A mean value of 9,22 mg/m².d which is significantly lower than the 1971 value of 46,06 mg/m².d. However, as stated before the mean values are impacted greatly by the predicted maximums at the source points. 75% of the predicted data is situated below 11,00 mg/m².d, which further indicates a much lower deposition compared to the 1971 data. The predicted maximum is 614,45 mg/m².d.

From the previous research by (Vaasma et al, [3]) we can now calculate the dose rate due to the deposited fly ash for any of the radionuclides in table 8. For ^{210}Pb this would yield an average dose rate of $9{,}22\,\frac{mg}{m^2.d}\,.\frac{204}{10^3}\frac{mBq}{mg} = 1{,}88\frac{mBq}{m^2.d}$ and a maximum dose rate of $614{,}45\,\frac{mg}{m^2.d}\,.\frac{204}{10^3}\frac{mBq}{mg} = 125{,}35\,\frac{mBq}{m^2.d}$. As can be seen in figure 21 the AEROPOL simulation of the year 1975 for dose rates due to the ^{210}Pb radionuclide is estimated to be lower (with a graphical maximum of 72,7 mBq/m².d). This might be due to the fact that the maximum value seems more wide spread and less concentrated compared to the WGBM model, a phenomena which also presents itself when comparing the other simulations.

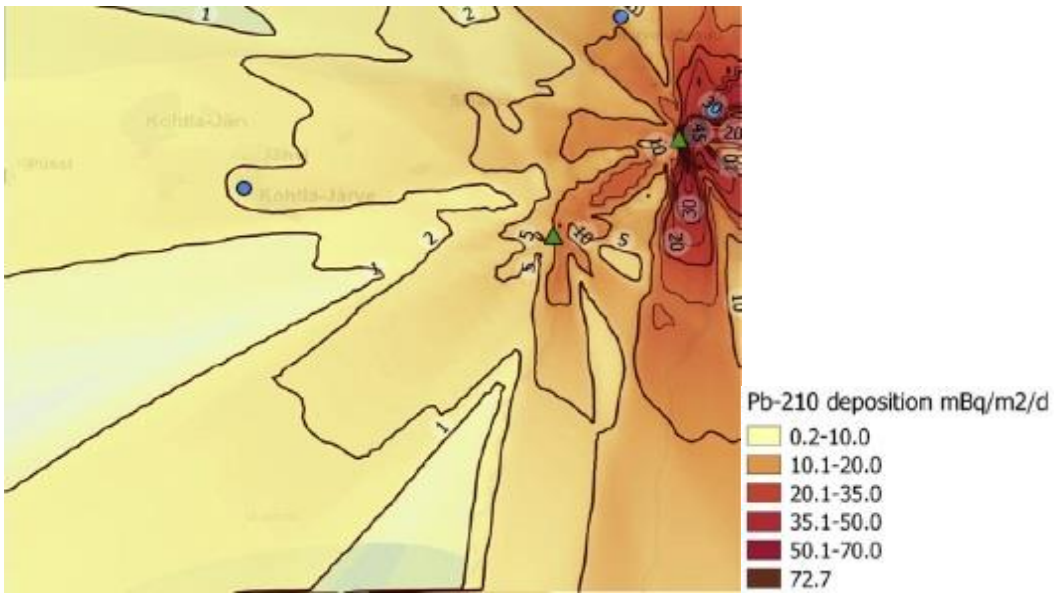

Figure 22: AEROPOL contour plot ('Heatmap') for the year 1975 modeling results for ^{210}Pb dose rate in mBq/m².d [3]

8.3.1.3. 1985

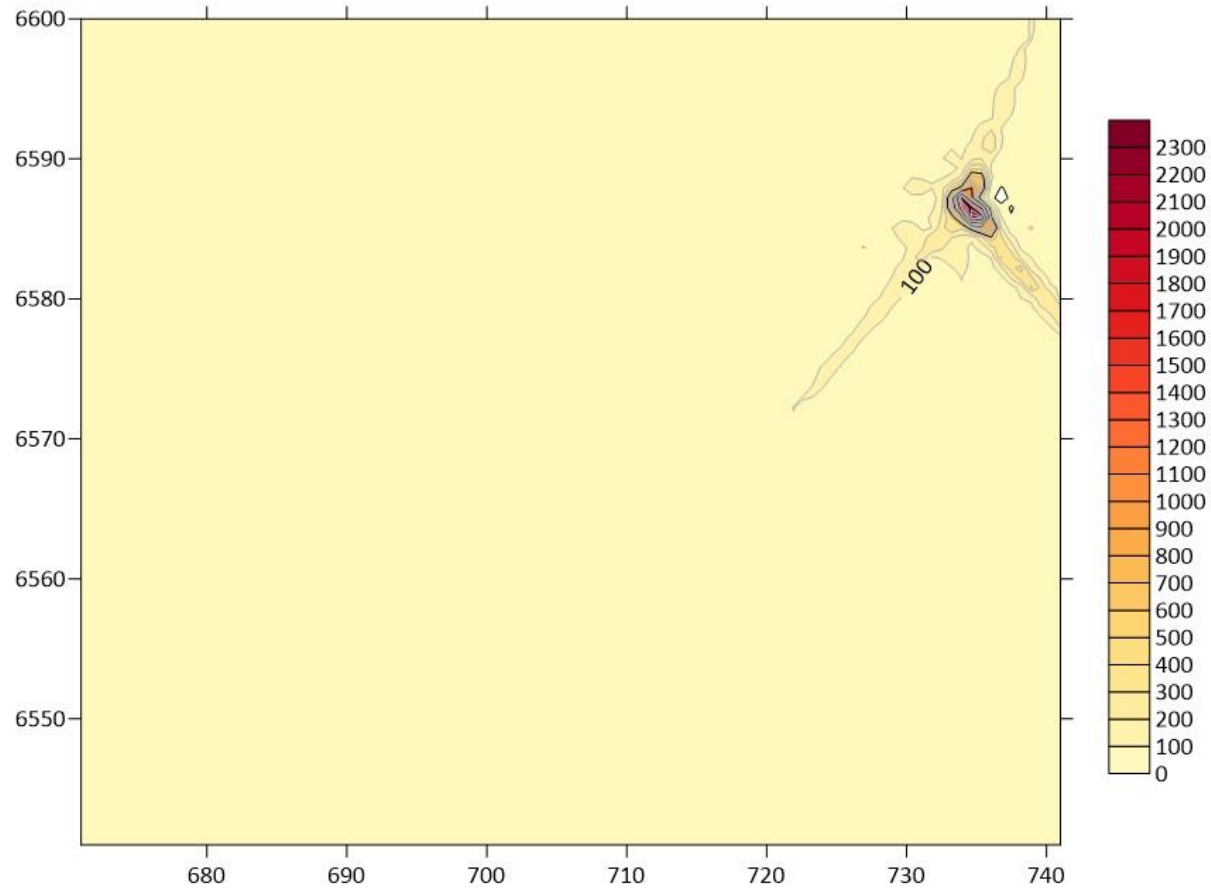

Figure 23: WGBM contour plot ('Heatmap') for the year 1985 modeling results in mg/m².d

The contour plot for the year 1985, displayed in figure 23, shows a very high maximum concentration, which skews the results heavily. In order to evaluate the low level dispersion spread a secondary plot was constructed with a set maximum, this resulted in figure 24.

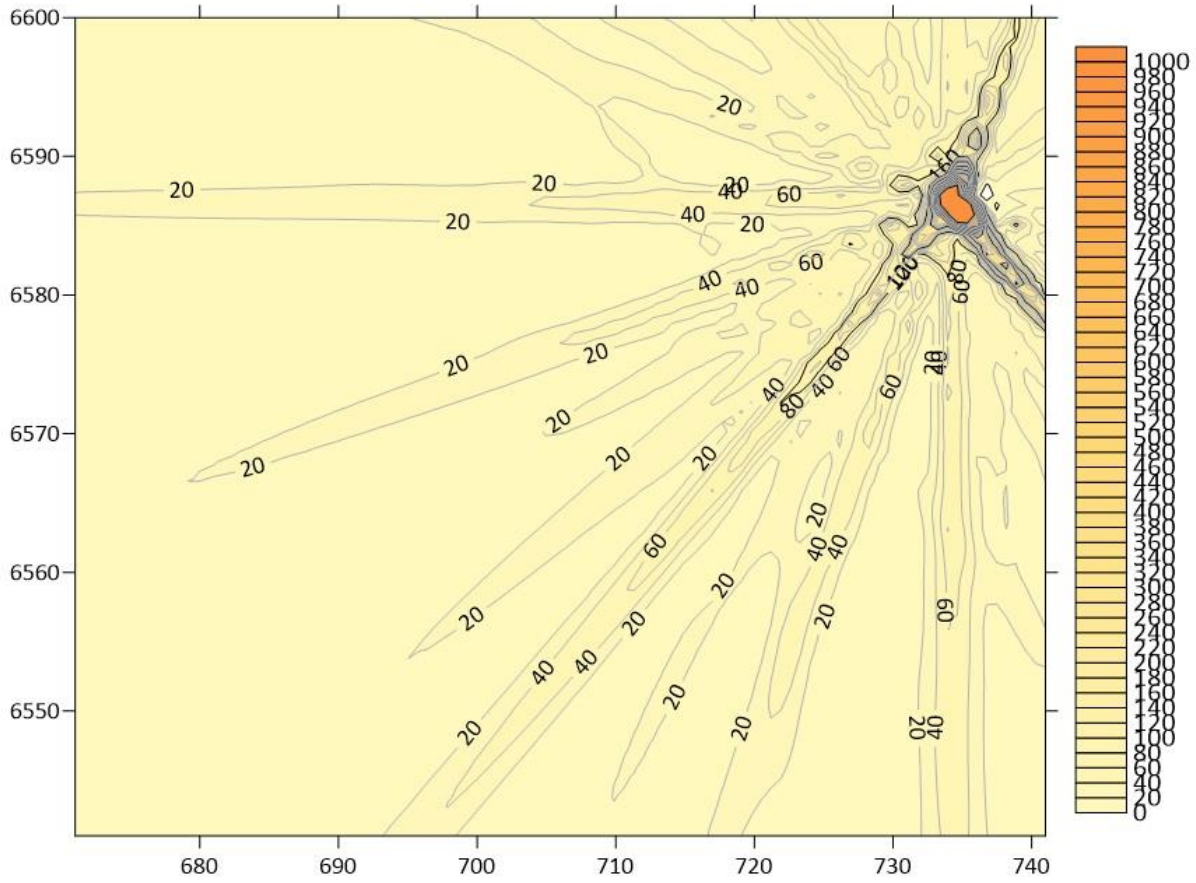

Figure 24: WGBM contour plot ('Heatmap') for the year 1985 modeling results in mg/m².d zoomed in order to see low value dispersions

As is the case for both the 1971 results as the 1975 results there is a centralized maximum to be found at the source point(s). There seems to be more variance in the lower value depositions, this may be due to the overall higher deposition prediction which causes negligible results in the 1971 and 1975 model to be higher and not negligible in the 1985 model. Statistical analysis yielded the following parameters. A mean of 23,85 mg/m².d, which is higher than the 1975 prediction which is curious as the overall consumption of shell oil is lower in 1985 than in 1975 as can be seen in figure 29 (section 8.4). The predicted maximum is 3818,70 mg/m².d which is abnormally high, this heavily influences the mean value as can be seen by the skewness factor which is 31,66. This means that most values are situated in the lower end of the distribution of values. This is also further demonstrated when evaluating the percentiles of the results. 99% of the results are situated below 146,29 mg/m².d, taking into account the total amount of predictions, there are only 43 points situated above 146,29 mg/m².d. Taking into account all these parameters a conservative maximum was chosen to be 614,45 mg/m².d, which is the maximum for the 1975 simulation. AEROPOL also predicts a much lower maximum than the 1985 model, namely around 330 mg/m².d. [3] The following dose rates to the environment can be assumed. An average dose rate due to the radionuclide ^{210}Pb of $23{,}85\,\frac{mg}{m^2.d}\,.\,204.\,10^{-3}\,\frac{mBq}{mg} = 4{,}87\,\frac{mBq}{m^2.d}$ and a conservative maximum dose rate of 125,35 mBq/m².d. As stated before this maximum dose rate is much higher than the predicted AEROPOL value, which is 67 mBq/m².d. [3] It is unsure why this abnormality is perceived as, even though the other simulations also deviate from the AEROPOL simulations, they do not deviate in such orders of magnitude. Since only the input parameters that change in this simulation is the measured meteorological parameters as well as the fly ash emission value (g/s) which is lower than the 1975 emission value. Taking into account all these factors deposition in 1985 should be marginally lower, since total fly ash emission was similar namely 174000 tons/year for 1975 and 163973 tons/year for 1985. [3]

8.3.1.4. 1995

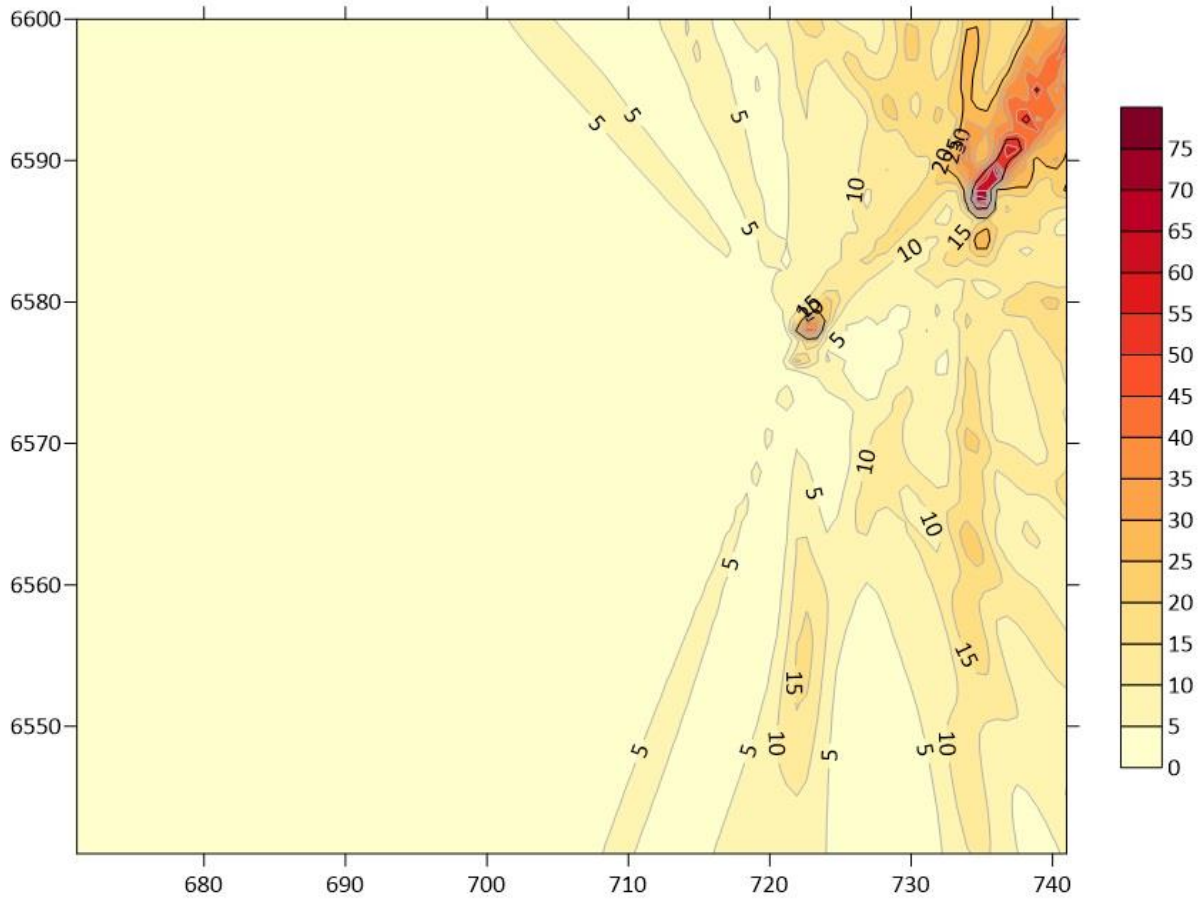

Figure 25: WGBM contour plot ('Heatmap') for the year 1995 modeling results in mg/m².d

As can be seen in figure 25 the overall deposition has been significantly reduced compared to the 1971, 1975 and 1985 results. This is due to the reduction in fly ash emissions which is comparatively, on average, 60% lower. The centralized maximum is less profoundly present in the contour plot, this may be due to the lower value of the maximum which does not skew the plot in the same way as in the previous ones. Statistical analysis revealed a mean value of 4,39 mg/m².d and a maximum value of 102,48 mg/m².d. This continues the trend set by the evaluation of the 1971's and 1975's prediction in which the mean progressively decreases and comparatively to the decrease in fly ash emission this is to be expected. 75% of the predicted deposition is situated below 6,16 mg/m².d, which also follows the tendency set by the 1971's and 1975's prediction. From the previous research by (Vaasma et al, [3]) we can now calculate the dose rate due to the deposited fly ash for any of the radionuclides in table 8. For ^{210}Pb this would yield an average dose rate of $4{,}39\frac{mg}{m^2.d} \cdot \frac{204}{10^3}\frac{mBq}{mg} = 0{,}90\frac{mBq}{m^2.d}$ and a maximum dose rate of $102{,}48\frac{mg}{m^2.d} \cdot \frac{204}{10^3}\frac{mBq}{mg} = 20{,}91\frac{mBq}{m^2.d}$. As can be seen in figure 26 the AEROPOL simulation of the year 1995 for dose rates due to the ^{210}Pb radionuclide is estimated to have a lower maximum, namely a graphical maximum of 17 mBq/m².d. [3] This might be due to the fact that the maximum value seems more wide spread and less concentrated compared to the WGBM model, a phenomena which also presents itself when comparing the other simulations. However, since 75% of the data from the WGBM simulation is situated below 6,16 mg/m².d the WGBM model does seem to have a good correlation with the AEROPOL model. This further emphasizes that the WGBM model preforms better in low deposition values (comparatively to AEROPOL) than it does in predicting maximum deposition values.

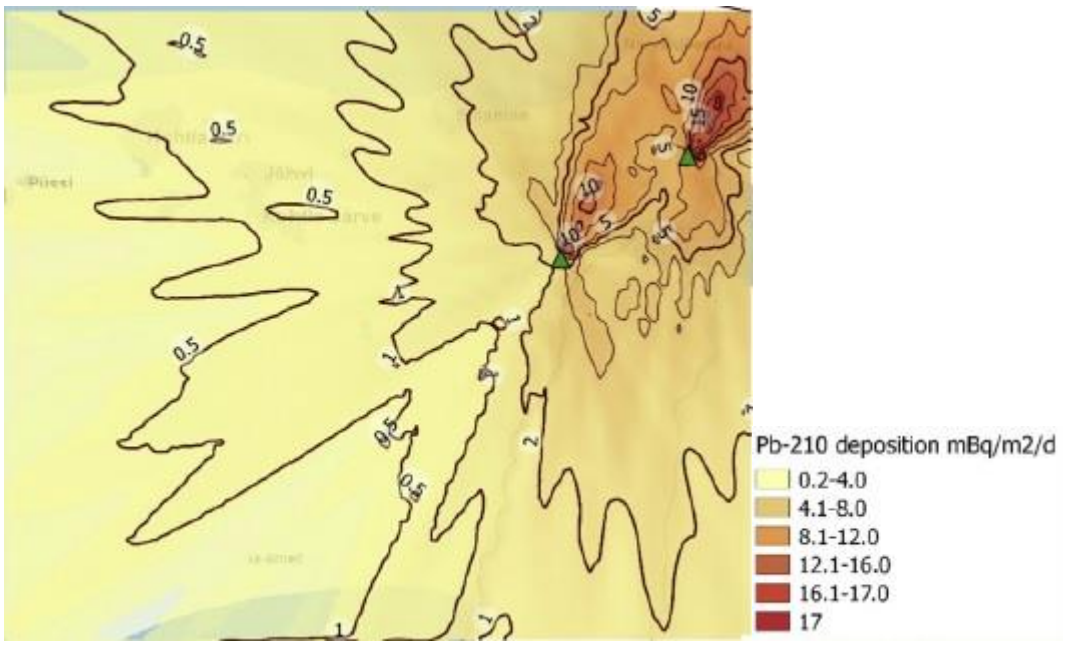

Figure 26: AEROPOL contour plot ('Heatmap') for the year 1995 modeling results for ^{210}Pb dose rate in mBq/m².d [3]

8.3.1.5. 1999

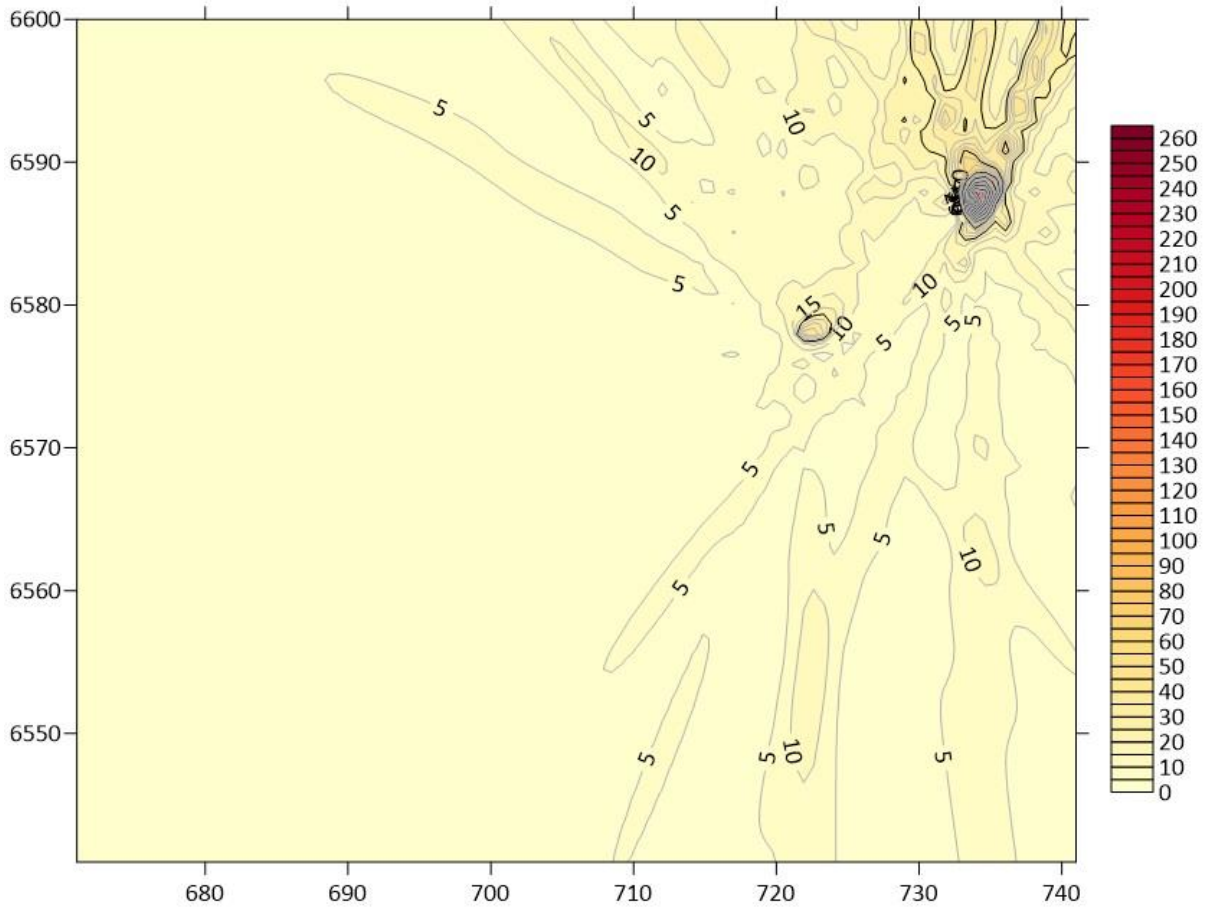

Figure 27: WGBM contour plot ('Heatmap') for the year 1999 modeling results in mg/m².d

Overall deposition seems to have been lowered even further, this is again to be expected since the fly ash emission is reduced even further compared to the 1995 emission, with a value of 12%. A more profound centralized maximum is observed. Statistical analysis of the 1995 simulated deposition gives us the following defining parameters. A mean value of 4,95 mg/m².d and a maximum value of 298,70 mg/m².d. In this case the mean value seems to be impacted less by the high maximum value predicted at the center of the point sources. Even though the statistical analysis predicts a higher mean value from the graphical analysis it is clear that overall deposition outside of the centralized maxima's is lower than in the 1995 model. The 1999's predicted maximum is more than double the 1995's predicted maximum, this could be due to a higher frequency in high rainfall values or coincidentally lower wind speeds when rainfall occurs. Both of these situations could cause a highly localized dose explaining the high maximum value (relative to the 1995's model). Other meteorological effects, such as certain stability classes occurring more or less, could also influence this. Even though the total fly ash emission in 1999 is 12% lower the effect this causes on the already very low deposition might be negated by the meteorological effects as stated before. The following dose rates to the environment can be assumed. An average dose rate due to the radionuclide ^{210}Pb of $4{,}95\frac{mg}{m^2.d}.204.10^{-3}\frac{mBq}{mg} = 1{,}01\frac{mBq}{m^2.d}$ and a conservative maximum dose rate of $298{,}70\frac{mg}{m^2.d}.\frac{204}{10^3}\frac{mBq}{mg} = 71{,}69\frac{mBq}{m^2.d}$. This maximum value is a lot higher than the AEROPOL predictions, which follow the declining tendency which was observed in the WGBM model in 1971, 1975 and 1995. [3]

8.4 AEROPOL

For illustration purposes a plot of the AEROPOL snow predictions compared to the measured snow deposition has been included below in figure 28.

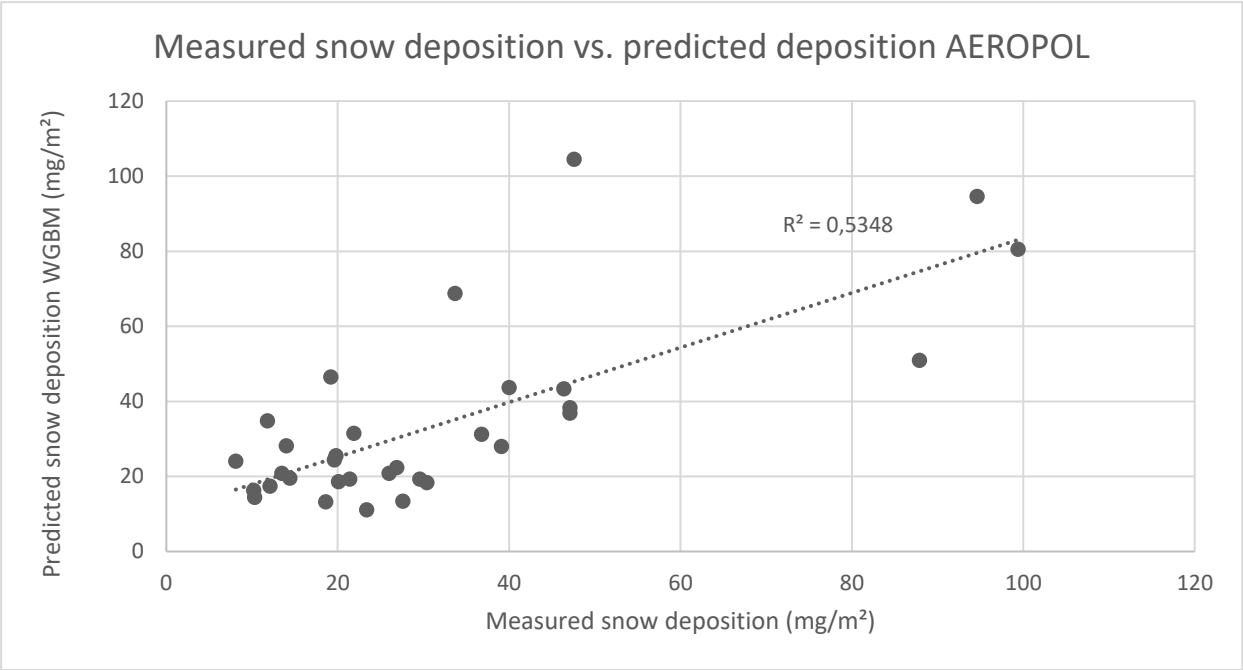

Figure 28: measured snow deposition vs. predicted deposition AEROPOL

AEROPOL predicts an average snow deposition of 33,80 mg/m².d which is a much better prediction than the other models.

AEROPOL also displayed a correlation to the WGBM results, making WGBM the closest related model to AEROPOL. This is odd as WGBM employs the Bultynck-Malet parametrization while AEROPOL uses the Pasquill-Gifford parametrization.

The AEROPOL study has shown that there is a significant variability in fly ash deposition ($\frac{mg}{m^2.d}$) throughout time. The largest depositions modeled have been during the 1970s and 1980s with up to 356 $mg.m^{-2}.d^{-1}$. This has a direct correlation with the fuel consumption during that time, which can be seen in figure 29, as well as a low efficiency of the filter systems. [3] Several radionuclide concentrations can be separately calculated as they are a function of the fly ash emission as well as the known activity concentration ratio between radionuclides. [3]

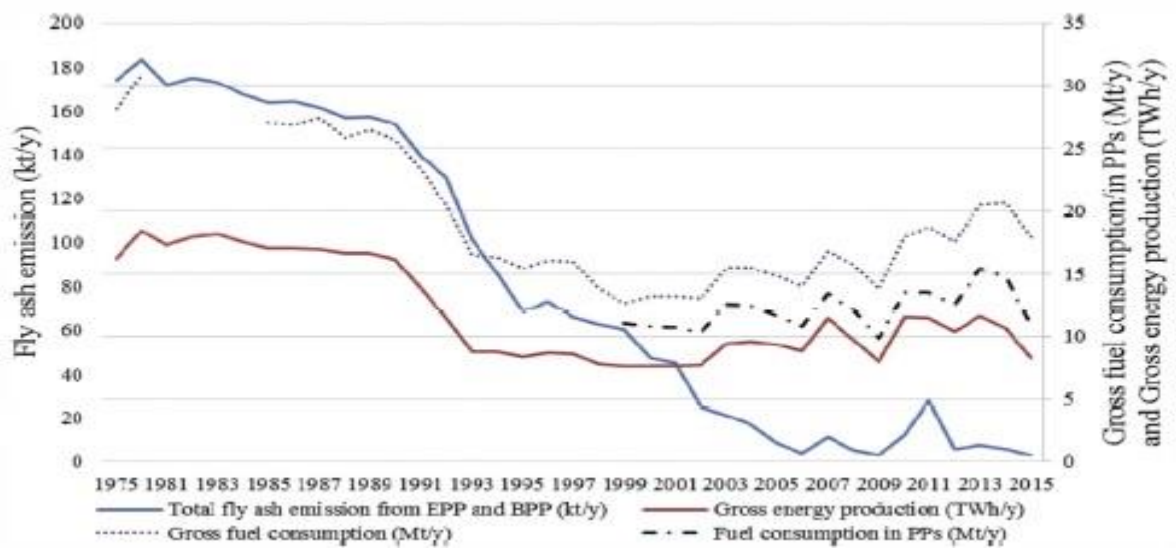

Figure 29: Comparison of overall oil shale consumption in Estonia and the consumption in the PPs; fly ash emissions and gross energy production by the PPs. Values only for the fly ash emission are shown on the left vertical axis. [3](p. 234)

8.4.1. Radiological burden on the environment

When estimating the radiological burden on the environment one must consider the half-life of the radionuclides present in the fly ash emissions. Radionuclides from the decay series from ^{238}U and ^{232}Th have a long half-life, which causes them to accumulate in the area surrounding the PPs. During the high shale oil consumption time (1970s & 1980s) the anthropogenic sources of ^{210}Pb contributed around 20-28% of natural background values; however, this has since then been lowered to below 1% nowadays. [3] Even though there is such a low contribution relative to the natural background values, the total radiological burden cannot be neglected as many radionuclides have long half-lives which makes them accumulate. It is also important to note that only the deposition has been considered in this study and other pathways of radiological doses should be considered (inhalation, ingestion,…). [3]

Both the AEROPOL and WGBM model predict a declining tendency in fly ash deposition, which is directly proportional to the radiological burden on the environment. However, WGBM consistently predicts higher (up to an order of magnitude) maximum concentrations, which are always situated at the source points.
AEROPOL studies showed a continued trend in which the predicted deposition, and thus dose rate, declined in the following years up to 2015. With dose rates being almost 60 times less in 2015 compared to the 1980s. [3]
Based on previous studies the background radiation due to ^{210}Pb, which is caused by the decay of radon, has been in the range of 92 and 133 $Bq/m^2.y$ in northern Estonia. Anthropogenic sources of ^{210}Pb thus constituted around 20-28% of natural background values in the 1980s, which was the high time of oil shale combustion. Nowadays the anthropogenic sources of ^{210}Pb contribute less than 1% of the natural background radiation. [3]

9. Conclusion

The original WESTIGAUSS code was successfully extended to include three new features: treatment of multiple sources (and therefore sources that are not centrally located), a rectangular grid (as well as the original polar one) and a time dependence of the source.
Three different models (based upon WESTIGAUSS) were simulated and compared to snow data in order to estimate their accuracy. Two of these models, based upon Paquill-Gifford parameterization, performed poorly with both models predicting much higher depositions than measurements showed. Correlation with the snow measurements were also less than expected. Both these models were discarded as potential models for further modeling due to this bad performance. The third model, based upon Bultynck-Malet parameterization, preformed comparatively better to the previous two models. It showed a positive and fairly good correlation to the snow measurements; however, it predicted consistently lower values. The AEROPOL model, which was used for comparison purposes, also showed a good positive correlation with the snow measurements. Since the third model preformed best comparatively to the snow measurements as well as compared to the AEROPOL model, this model was chosen to conduct additional simulations.
The years chosen for modeling included 1971, 1975, 1985, 1995 and 1999. Moderate agreement was found between the WESTIGAUSS Bultynck-Malet model's results and the AEROPOL model's results. With the WESTIGAUSS model predicting a decline in deposition throughout the years, which was first predicted by the AEROPOL model. However, the WESTIGAUSS model's prediction for maximum concentration was found to be consistently higher than the AEROPOL model's prediction. This skewed the mean value prediction for the WESTIGAUSS model to a higher value. Even though the WESTIGAUSS model predicted a consistently higher maximum concentration, it also predicted this maximum concentration to be less spread out over the environment and instead to be concentrated to the source points. Mean and maximum concentrations predicted by the WESTIGAUSS model were the following:

- 1971 : mean = 46,06 mg/m².d & max = 1421,73 mg/m².d;
- 1975 : mean = 9,22 mg/m².d & max = 614,45 mg/m².d;
- 1985 : mean = 23,85 mg/m².d & max = 3818,70 mg/m².d;
- 1995 : mean = 4,39 mg/m².d & max = 102,48 mg/m².d;
- 1999 : mean = 4,59 mg/m².d & max = 298,70 mg/m².d.

The year 1985 displayed a very high maximum value, which could be explained by the WESTIGAUSS tendency to overpredict maximum values. This raised the mean value for the year 1985 significantly; however, further analysis showed low level dispersions to be as expected. For this reason these predicted values were not used in the radiological impact assessment. 1971, 1975 and 1995 showed a declining tendency in deposition values, which is in accordance to the AEROPOL predictions. 1999 showed a slight increase in deposition compared to the 1995 results; however, it is observed that this mean value is again influenced heavily by the maximum value. Further graphical analysis of the year 1999 showed that on average lower value depositions were predicted, but a higher maximum value was due to a less spread out maximum.
In order to determine the radiological burden on the environment one particular radionuclide was chosen, namely ^{210}Pb. This radionuclide was chosen in accordance with the AEROPOL research as well as multiple other studies. A constant activity concentration was used, namely 204 Bq/kg, in order to estimate the dose rate deposition. Since the WESTIGAUSS model preformed good in comparison to the AEROPOL model, displaying the same tendency in steady decline of deposition (with the exception of the year 1985), results were similar in the radiological burden on the environment. As shown by the AEROPOL research the anthropogenic sources of ^{210}Pb constituted 20-28% of the natural background value (92-133 Bq/m².y) in the 1970's and 1980's. The same is demonstrated by the WESTIGAUSS model, as well as the steady decline in dose rate deposited due to fly ash deposition. WESTIGAUSS did predict higher maximum values consistently throughout all simulations, which may be due to the Bultynck-Malet parametrization; however, this cannot be said with absolute certainty.

Bibliography

[1] "SCK-CEN : Brief Presentation," SCK-CEN, [Online]. Available: http://sckcen.be/en/About/Introduction. [Accessed 12 10 2017].

[2] "Organisation Chart," SCk-CEN, [Online]. Available: http://intern.sckcen.be/organigram/. [Accessed 12 10 2017].

[3] T. Vaasma, M. Kaasik, J. Loosaar, M. Kiisk and A. H. Tkaczyk, "Long-term modelling of fly ash and radionuclide emissions as well as deposition fluxes due to the operation of large oil shale-fired power plants," *Elsevier,* no. 178-179, pp. 232-244, 2017.

[4] G. Hoek, R. M. Krishnan, R. Beelen, A. Peter, B. Ostro and B. Brunekreef, "Long-term air pollution exposure and cardio-respiratory mortality: a review," *Environmental Health,* no. 12:43, 2013.

[5] K. Isakar, M. Kiisk, E. Realo and S. Suursoo, "Lead-210 in the atmospheric air of North and South Estonia: long-term monitoring and back-trajectory calculations," *Proceedings of the Estonian Academy of Sciences,* no. 65, pp. 442-451, 2016.

[6] T. Vaasma, M. Kiisk, T. Meriste and A. H. Tkaczyk, "The enrichment behavior of natural radionuclides in pulverized oil shale-fired power plants," *Elsevier,* no. 138, pp. 427-433, 2014.

[7] World Nuclear Association, "World Nuclear Association," May 2018. [Online]. Available: http://www.world-nuclear.org/information-library/safety-and-security/radiation-and-health/naturally-occurring-radioactive-materials-norm.aspx. [Accessed 3 June 2018].

[8] J. Garner, J. Cairns and D. Read, "NORM in the East Midland' oil and gas producing region of the UK," *Elsevier - Journal of Environmental Radioactivity,* no. 150, pp. 49-56, 2015.

[9] A. Srivastava, S. Lahiri, M. Maiti, F. Knolle, F. Hoyler, U. W. Scherer and E. W. Schnug, "Study of naturally occurring radioactive material (NORM) in top soil of Punjab State from the North Western part of India," *J Radioanal Nucl Chem,* no. 302, pp. 1049-1052, 2014.

[10] S. Uddin, M. Behbehani, A. Aba and A. N. Al Ghadban, "Naturally Occurring Radioactive Material (NORM) in seawater of the northern Arabian Gulf – Baseline measurements," *Elsevier - Marine Pollution Bulletin,* no. 123, pp. 365-372, 2017.

[11] L. Vallner, O. Gavrilova and R. Vilu, "Environmental risks and problems of the optimal management of an oil shale semi-coke and ash landfill in Kohtla-Järve, Estonia," *Elsevier,* no. 524-525, pp. 400-415, 2015.

[12] L. A. Anuela-Tapola, F. J. Frandsen and E. K. Häsänen, "Trace metal emissions from the Estonian oil shale fired power plant," *Elsevier - Fuel Processing Technology,* no. 57, pp. 1-24, 1998.

[13] E. Realo, K. Realo and J. Jogi, "Releases of Natural Radionuclides from Oil-shale-fired power plants in Estonia," *Elsevier,* no. 33, pp. 77-89, 1996.

[14] J. E. Martin, Physics for Radiation Protection, Weinheim: Wiley-VCH, 2006.

[15] J. Duyzer, D. van den Hout and v. R. S. Zandveld Peter, "Representativeness of air quality monitoring networks," *Elsevier,* pp. 88-101, 31 December 2014.

[16] J. B. Lewis, N. E. Onder and A. A. Prudil, "Fundamentals of Nuclear Engineering," in *Nuclear Reactor Safety*, John Wiley & Sons, 2017, pp. 645-660.

[17] S. Alessandrini, E. Ferrero and D. Anfossi, "A new Langragian method for modelling the buoyant plume rise," *Eslevier - Atmospheric Environment*, no. 77, pp. 239-249, 2013.

[18] D. Liu, Environmental Engineer' Handbook : Second Edition, Taylor &Amp; Francis Inc, 1997.

[19] J. Ruts and A. Sohier, Noodplan Kempen, Mol: SCK-CEN, 1995.

[20] R. R. Burton, "Atmospheric Dispersion," Institute for Atmospheric Science.

[21] D. L. N. e. E. Vlaamse Overheid, "IMPACT - Imission Prognosis Air Concentration Tool," Heirman, Jean-Pierre, Brussel, 2017.

[22] T. Vidmar, J. Camps, D. Braeckers and G. Olyslager, "WESTIGAUSS – AN ATMOSPHERIC DISPERSION MODELLING AND ENVIRONMENTAL IMPACT ASSESSMENT TOOL FOR NUCLEAR INSTALLATIONS," in *14th Conference on Harmonisation within Atmospheric Dispersion Modelling for Regulatory Purposes*, Kos, Greece, 2011.

[23] G. A. Davidson, "A Modified Power Law Representation of the Pasquill-Gifford Dispersion Coefficients," *Journal of the Air & Waste Management Association* , no. 40:8, pp. 1146-1147, 1990.

[24] P. A. Davis, "Tritium Transfer Parameters for the Winter Environment," *Elsevier*, no. 36, pp. 177-196, 1997.

[25] S. M. Vakulovskii, M. A. Novitskii, N. F. Mazurin, E. G. Tertyshnik and L. M. Khachaturova, "Preliminary Results of Modeling Studies on Washout of Stable and Radioactive Analogs of 90-Sr and 137-Cs from Snow-Covered Areas," *Russian Meteorology and Hydrology*, no. 32, pp. 508-513, 2007.

[26] S. (. source), "Reactor Licensing," in *Reactor Licensing* , pp. 630-676.

[27] K. S. Krane, Introductory Nuclear Physics, United States of America: John Wiley & Sons, 1988.

[28] R. R. Burton, "Atmospheric dispersion," Leeds, [Online]. Available: http://homepages.see.leeds.ac.uk/~lecrrb/dispersion/index5.html. [Accessed 22 Januari 2018].

Auteursrechtelijke overeenkomst

Ik/wij verlenen het wereldwijde auteursrecht voor de ingediende eindverhandeling:
Radiological and non-radiological environmental impact assessment of Estonian power plants

Richting: **master in de industriële wetenschappen: nucleaire technologie-milieutechnologie-radiochemie**
Jaar: **2018**

in alle mogelijke mediaformaten, - bestaande en in de toekomst te ontwikkelen - , aan de Universiteit Hasselt.

Niet tegenstaand deze toekenning van het auteursrecht aan de Universiteit Hasselt behoud ik als auteur het recht om de eindverhandeling, - in zijn geheel of gedeeltelijk -, vrij te reproduceren, (her)publiceren of distribueren zonder de toelating te moeten verkrijgen van de Universiteit Hasselt.

Ik bevestig dat de eindverhandeling mijn origineel werk is, en dat ik het recht heb om de rechten te verlenen die in deze overeenkomst worden beschreven. Ik verklaar tevens dat de eindverhandeling, naar mijn weten, het auteursrecht van anderen niet overtreedt.

Ik verklaar tevens dat ik voor het materiaal in de eindverhandeling dat beschermd wordt door het auteursrecht, de nodige toelatingen heb verkregen zodat ik deze ook aan de Universiteit Hasselt kan overdragen en dat dit duidelijk in de tekst en inhoud van de eindverhandeling werd genotificeerd.

Universiteit Hasselt zal mij als auteur(s) van de eindverhandeling identificeren en zal geen wijzigingen aanbrengen aan de eindverhandeling, uitgezonderd deze toegelaten door deze overeenkomst.

Voor akkoord,

Slechten, Wouter

Datum: **6/06/2018**